Molecular Therapy
Nucleic Acids
Original Article

Subretinal gene therapy delays vision loss in a Bardet-Biedl Syndrome type 10 mouse model

Ying Hsu,[1] Sajag Bhattarai,[1] Jacob M. Thompson,[1] Angela Mahoney,[1] Jacintha Thomas,[1] Sara K. Mayer,[1,3] Poppy Datta,[1] Janelle Garrison,[2] Charles C. Searby,[2] Luk H. Vandenberghe,[4] Seongjin Seo,[1] Val C. Sheffield,[1,2] and Arlene V. Drack[1]

[1]Department of Ophthalmology and Visual Sciences, University of Iowa, Iowa City, IA, USA; [2]Department of Pediatrics, University of Iowa, Iowa City, IA, USA; [3]Interdisciplinary Graduate Program in Genetics, University of Iowa, Iowa City, IA, USA; [4]Massachusetts Eye and Ear, Grousbeck Gene Therapy Center, Harvard Medical School, Boston, MA, USA

Blindness in Bardet-Biedl syndrome (BBS) is caused by dysfunction and loss of photoreceptor cells in the retina. *BBS10*, mutations of which account for approximately 21% of all BBS cases, encodes a chaperonin protein indispensable for the assembly of the BBSome, a cargo adaptor important for ciliary trafficking. The loss of BBSome function in the eye causes a reduced light sensitivity of photoreceptor cells, photoreceptor ciliary malformation, dysfunctional ciliary trafficking, and photoreceptor cell death. Cone photoreceptors lacking BBS10 have congenitally low electrical function in electroretinography. In this study, we performed gene augmentation therapy by injecting a viral construct subretinally to deliver the coding sequence of the mouse *Bbs10* gene to treat retinal degeneration in a BBS10 mouse model. Long-term efficacy was assessed by measuring the electrical functions of the retina over time, imaging of the treated regions to visualize cell survival, conducting visually guided swim assays to measure functional vision, and performing retinal histology. We show that subretinal gene therapy slowed photoreceptor cell death and preserved retinal function in treated eyes. Notably, cone photoreceptors regained their electrical function after gene augmentation. Measurement of functional vision showed that subretinal gene therapy provided a significant benefit in delaying vision loss.

INTRODUCTION

Bardet-Biedl syndrome (BBS) is a model ciliopathy. In this disorder, mutations in genes important for maintaining the function of cilia—"the antenna of the cell"—cause cellular dysfunction in multiple cell types, leading to obesity, polydactyly, renal failure, and blindness. Many of these mutations disable the function of a protein complex called the BBSome, which acts as a cargo adaptor to the intraflagellar transport (IFT) complex, expands the cargo range of IFT in ciliary trafficking,[1] and regulates the movement of cargo proteins in and out of cilia.[2] In the retina, the primary cilium of the photoreceptor has evolved into a structure specializing in phototransduction called the outer segment, which occupies up to 40% of the photoreceptor cell volume.[3] These enlarged cilia of photoreceptors require more active protein trafficking for their maintenance compared with the primary cilia of other cell types, and they in turn render the photoreceptors particularly vulnerable to mutations that disrupt ciliary transport or function. The disruption of BBSome function leads to the inundation of photoreceptor outer segments by more than 100 different proteins normally found in other parts of the cell, including syntaxin-3 (STX3).[4] Cellular stress caused by protein mislocalization contributes to photoreceptor cell death in BBS.[4] In addition, disrupting the BBSome causes malformation of the photoreceptor outer segment prior to degeneration,[5] increased cellular stress,[6] and eventually photoreceptor cell death, leading to blindness.[5,7-10] Developing treatments for preventing blindness in BBS is a major research focus in the last decade.

BBS is a genetically heterogeneous disorder, with at least 22 causative genes known to date,[11] and mutations in *BBS10* are the second most common cause of BBS next to *BBS1*. Mutations in *BBS10* account for approximately 21% of BBS cases.[12] Although not a part of the BBSome complex, BBS10 is indispensable for BBSome assembly.[13] Therefore, intact ciliary transport requires a functional *BBS10* gene. BBS10 belongs to the group II chaperonins and possesses a conserved ATP-binding site for ATP hydrolysis, suggesting that it may be a catalytically active enzyme.[12] BBS10 forms a complex with BBS6, BBS12, and six chaperonin-containing TCP1 (CCT) proteins and interacts with BBSome components BBS2 and BBS7 to facilitate the BBSome assembly.[13] Mouse models with defective *Bbs10* function have BBS phenotypes.[14] *Bbs10*$^{-/-}$ mice have classical BBS features including obesity, male infertility, and a progressive loss of photoreceptor cells in the eye.[14] By 6 months of age, *Bbs10*$^{-/-}$ mice exhibit severe visual impairment in both light and dark conditions as determined by

Received 11 May 2022; accepted 9 December 2022;
https://doi.org/10.1016/j.omtn.2022.12.007.

Correspondence: Arlene V. Drack, Department of Ophthalmology and Visual Sciences, University of Iowa, Iowa City, IA, USA.
E-mail: arlene-drack@uiowa.edu

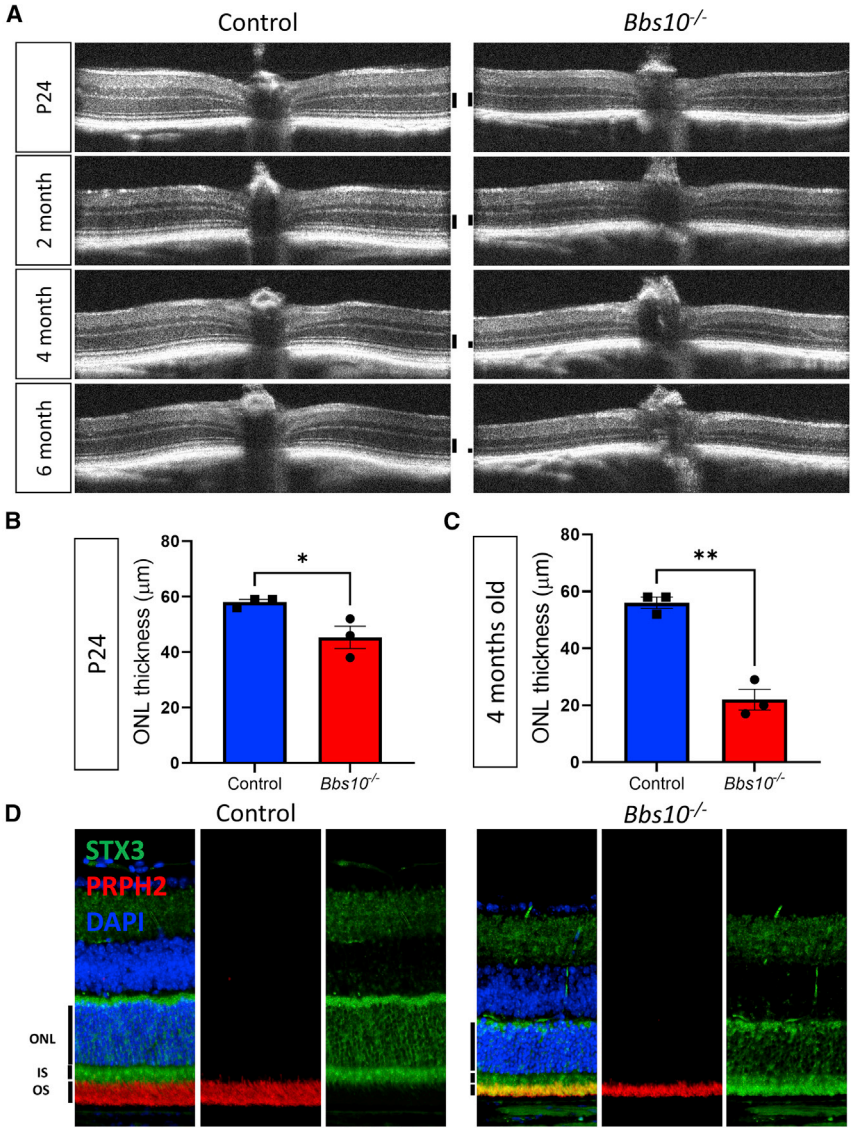

Figure 1. Progression of retinal degeneration in untreated *Bbs10*$^{-/-}$ mice

Bbs10$^{-/-}$ mice have progressive loss of photoreceptor cells. (A) OCT images of a *Bbs10*$^{-/-}$ mouse (right) and a wild-type or heterozygous control littermate (left) are shown, and the outer nuclear layers (ONLs) are indicated by a black solid bar next to the OCT image. (B) At P24, the thickness of the ONL in *Bbs10*$^{-/-}$ mice is 83% of that in their control littermates. (C) By 4 months of age, more than half of the retinal photoreceptors are lost in the retinas of *Bbs10*$^{-/-}$ mice. Statistical comparisons for ONL thicknesses were performed using two-tailed t tests. The error bar represents standard error of the mean. (D) STX3, a SNARE protein normally confined to the photoreceptor inner segment (IS), mislocalizes to the outer segment (OS) in *Bbs10*$^{-/-}$ mice at P21.

electroretinography (ERG) and the visually guided swim assay.[14] The visually guided swim assay, in particular, provides a quantitative metric of rodent visual navigation. By 7–8 months of age, nearly all the photoreceptors are lost in the retinas of *Bbs10*$^{-/-}$ mice.[14] Therefore, *Bbs10*$^{-/-}$ mice recapitulate retinal degeneration and vision loss seen in BBS10 patients. Of note, prior to notable retinal degeneration, *Bbs10*$^{-/-}$ mice already possess low, barely recordable cone electrical function in ERG, which is likely caused by the mislocalization of cone opsins and the loss of transducins in the absence of BBSome function.[14] It remains to be determined whether the early absence of cone function despite the presence of cone cells can be amended by the restoration of *Bbs10* gene function. *Bbs10*$^{-/-}$ mice offer an animal model for evaluating the long-term efficacy of a subretinal gene therapy to prevent blindness in BBS10 patients.

The potential of using gene augmentation therapy to treat BBS has been demonstrated. In a proof-of-concept study where the *Bbs8* gene is temporarily disabled by a gene trap, we showed that the activation of the *Bbs8* gene in young animals by removing the gene trap prevents photoreceptor cell death and restores photoreceptor ciliary structure and function in the eye.[5]

To test whether blindness in BBS type 10 (BBS10) can be treated with retinal gene augmentation therapies, we conducted a preclinical study in a mouse model of BBS10. In this study, we treated 23-31-day-old *Bbs10*$^{-/-}$ mice with a subretinal injection of an adeno-associated virus (AAV) containing the coding sequence of the mouse *Bbs10* gene driven by a cytomegalovirus (CMV) promotor. We evaluated retinal electrical function and the integrity of retinal layers in treated regions over time up to 10–12 months after treatment to assess long-term efficacy. We also performed a vision assay at two different time points after treatment to determine if gene therapy provided benefits in delaying vision loss in the disease course of BBS10. Laboratory mice have averaged life spans of 2–3 years.[15,16] The experimental time course chosen in this study reflects the effect of early intervention on BBS10 disease trajectory over a significant portion of the lives of laboratory mice.

RESULTS

Bbs10 knockout mice have progressive loss of photoreceptors

Bbs10$^{-/-}$ mice have progressive retinal degeneration characterized by the gradual loss of photoreceptor cells (Figure 1A). At postnatal day (P) 24, when the retina has completed its maturation process in mice, the thickness of the outer nuclear layer (ONL) in *Bbs10*$^{-/-}$ mice was 84.5% of that of their wild-type or heterozygous littermate controls, suggesting the presence of a mild degeneration at this age (controls, 58.0 ± 1.0 μm, n = 3; *Bbs10*$^{-/-}$, 49.0 ± 4.06 μm, n = 3; $p < 0.05$; Figure 1B).

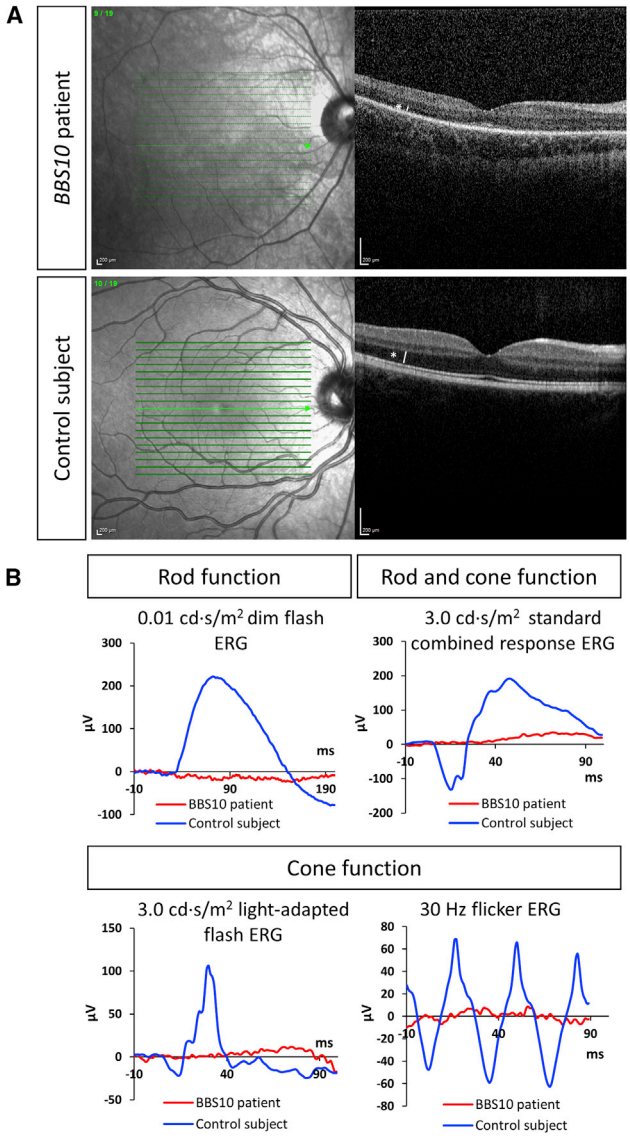

Figure 2. Patient with biallelic *BBS10* mutations has rapid retinal degeneration

(A) OCT images are shown for an 8-year-old patient with biallelic mutations in *BBS10* (p.Leu414Ser, p.Cys91Leufs*5) and a 12-year-old control subject. The thickness of the ONL in the BBS10 patient is 36.1% of that in the control subject. In the OCT images, the ONL is marked by an asterisk, and the white line next to the asterisk indicates the thickness of the ONL. The positions of the scans displayed are indicated by thearrowed green line in the fundus images. (B) ERG waveforms of an 8-year-old BBS10 patient and a 10-year-old control subject are shown for the dark-adapted 0.01 cd s/m^2 dim flash, dark-adapted 3.0 cd s/m^2 standard combined response, the light-adapted 3.0 cd s/m^2 bright flash, as well as the light-adapted 30-Hz flicker response.

By 4 months of age, ONL thicknesses in *Bbs10*$^{-/-}$ mice were 39.3% of that in their heterozygous or wild-type littermates (controls, 56.0 ± 2.0 μm, n = 3; *Bbs10*$^{-/-}$, 22.0 ± 3.61 μm, n = 3; $p < 0.005$; Figure 1C). To compare the disease progression in humans and mice, we show optical coherence tomography (OCT) images of a patient with biallelic mutations in *BBS10* (p.Leu414Ser [NCBI: NP_078961.3; ClinVar: NM_024685.4:c.1241T>C; dbSNP: rs786204575] and p.Cys91Leufs*5 [NCBI: NP_078961.3; ClinVar: NM_024685.4:c.271dup; dbSNP: rs549625604]). Leu414Ser is a missense mutation classified as pathogenic or likely pathogenic in the Clinvar database, and p.Cys91Leufs*5 is a common indel mutation that causes an early frameshift in *BBS10*. This patient has been previously reported.[17] At 8 years of age, the ONL thickness of this patient is approximately 36.1% of that in a control subject (ONL in patient, 41.6 μm; ONL in control subject, 115.3 μm; Figure 2A). Although mouse age and human age are not correlated in a linear fashion, the degree of ONL degeneration observed in the patient is roughly comparable with that observed in 4-month-old *Bbs10*$^{-/-}$ mice. This BBS10 patient, at age 8 years, has non-recordable waveforms in all ERG measures tested, including rod-specific 0.01 cd s/m^2 dim flash, 3.0 cd s/m^2 standard combined response ERG, and the cone-specific 3.0 cd s/m^2 bright flash as well as the 30-Hz flicker response (Figure 2B). *Bbs10*$^{-/-}$ mice have congenitally absent or low cone photoreceptor electrical function, and rod ERGs become non-recordable between 6 and 9 months of age.[14] Together, these data suggest that the lack of BBS10 causes low photoreceptor function and progressive retinal degeneration, and the disease phenotypes observed in humans are recapitulated in the BBS10 mouse model.

In normal photoreceptors, the BBSome functions in protein transport. Without the proper functioning of the BBSome, more than 100 proteins, including STX3, flood the photoreceptor outer segment compartment, causing cellular stress.[4] As a soluble N-ethylmaleimide attachment protein receptor (SNARE) protein, STX3 is normally enriched in the photoreceptor inner segment and the synaptic layer. In contrast, in BBS mouse models lacking adequate BBSome function, including in *Bbs1*$^{M390R/M390R}$, *Bbs4*$^{-/-}$, and *Bbs8*$^{-/-}$ mice, STX3 mislocalizes to the photoreceptor outer segment, a sign of impaired ciliary trafficking.[5,18] We examined STX3 localization in the retinas of *Bbs10*$^{-/-}$ mice and their littermate controls at P21. The photoreceptor outer segments were labeled using an anti-rhodopsin (RHO) antibody. In *Bbs10*$^{-/-}$ retinas, STX3 immunoreactivity overlaps with that from RHO, representing the mislocalization of STX3 to the photoreceptor outer segments (Figure 1D). STX3 shows normal distribution in retinas of control littermates (Figure 1D). Therefore, loss of BBS10 leads to STX3 mislocalization to the photoreceptor outer segment, similar to that observed in mutant models of the BBSome, suggesting that loss of BBS10 disrupts BBSome-dependent ciliary trafficking.

AAV2/Anc80 transduces photoreceptors and RPE after subretinal delivery

For testing subretinal gene therapy in this preclinical mouse model, we used the AAV2/Anc80 viral vector, the predicted closest common ancestor of AAV serotypes 1–3 and 6–9,[19] to deliver the target gene to the retina. This viral vector possesses high transduction efficiency for the photoreceptors and the retinal pigment epithelium (RPE).[19] To visualize the tropism of this AAV, an expression cassette encoding the green fluorescent protein (GFP), driven by a CMV promoter, was packaged into the AAV2/Anc80 viral capsid and delivered

subretinally into 1-month-old heterozygous and wild-type mice. During subretinal injection, the injection of fluid into the subretinal space creates a localized subretinal bleb, where a part of the retina is detached and elevated and the retina and RPE are temporarily separated to accommodate the injected fluid. Mice received 2×10^9 viral genomes (vg) or 8×10^9 vg of AAV2/Anc80-*CMV-GFP* per eye, and the sizes of the subretinal blebs raised were recorded at the time of injection. To visualize the transduced areas, fluorescence fundoscopy was performed to capture the fluorescence from GFP 2 weeks after subretinal injection (Figure S1). In mice with "excellent" blebs, defined by a temporary elevation of greater than 50% of total retinal area, GFP fluorescence was observed in the majority of the retinal area imaged (Figure S1). In mice with "moderate-sized" blebs, defined by the temporary elevation of approximately 25% of the total retinal area, fluorescence fundoscopy showed that the area expressing GFP was correspondingly smaller, and typically confined to a quadrant of the retina (Figure S1). In mice with "small" blebs, defined by the temporary elevation of less than 25% of the total retinal area at time of injection, the GFP-expressing regions were limited to defined foci (Figure S1). In the eye shown in Figure S1, which had a small bleb, visible fluid reflux from the syringe was also noted at time of injection. In the fluorescence fundus image, the observation of elongated, GFP-expressing fibers could potentially be caused by the escape of the injected vector into the intravitreal space, thereby transducing ganglion cells (Figure S1). Overall, the sizes of the subretinal blebs observed through the operating microscope at time of injection corresponded to the sizes of GFP-expressing regions seen in fluorescence fundoscopy. For the remainder of this study, animals with small or no subretinal blebs at the time of injection were excluded from the study.

To determine whether the observed GFP fluorescence in fluorescence fundoscopy arises from the transduction of retinal photoreceptor cells, we performed fluorescence microscopy using cryosections of these retinas 1 month after injection of AAV2/Anc80-*CMV-GFP*. In an animal that received 2×10^9 vg of AAV2/Anc80-*CMV-GFP* and had a moderate-sized bleb after injection, fluorescence images show that, near the injection site (Figure S1B, arrow), greater than 50% of photoreceptors strongly express GFP, indicating that this viral vector efficiently transduces photoreceptor cells. Far away from the injection site (Figure S1B, arrowhead), presumably at a location outside of the raised bleb, few photoreceptors express GFP. The percentages of GFP-expressing photoreceptors decline as a function of the distance from the injection site. Numerous RPE cells that strongly express GFP are also observed (Figure S1C, arrowhead), along with RPE cells that do not (Figure S1C, arrow), and the proportion of transduced versus non-transduced RPE cells is also a function of the distance to the site of injection. Some inner retinal cells also express GFP (Figure S1B, asterisk). These patterns are not observed in the uninjected, contralateral eye, even though the scleral tissue exhibits some degree of autofluorescence (Figure S2). These observations indicate that the AAV2/Anc80 viral vector effectively transduces photoreceptor cells and the RPE, as well as some cells in the inner retina of the mouse eye, when delivered subretinally.

To test whether gene augmentation therapy using the AAV2/Anc80 viral vector could treat retinal degeneration in BBS10, we packaged a gene expression cassette containing the CMV promoter, the coding sequence of the mouse *Bbs10* gene, and a bovine growth hormone (bGH) transcription termination signal into the AAV2/Anc80 viral vector (Figure S3).

Subretinal delivery of AAV2/Anc80-CMV-mBbs10 does not cause adverse effects

To determine whether the injection of AAV2/Anc80-*CMV-mBbs10* causes adverse effects, wild-type or heterozygous mice were subretinally injected with this vector at 8×10^9 vg and compared with mice that received a subretinal injection of the delivery buffer only (sham injection), and completely untreated eyes. ERG was performed at 1, 2, 3, and 5 months after treatment. Injection of AAV2/Anc80-*CMV-mBbs10* did not adversely influence the ERG values of treated eyes compared with sham-injected eyes and uninjected eyes (Figure S4). These experiments show that subretinal delivery of AAV2/Anc80-*CMV-mBbs10* did not cause adverse events.

Subretinal gene therapy of Bbs10 delays the loss of rod photoreceptor function in treated eyes

The AAV2/Anc80-*CMV-mBbs10* viral vector was subretinally delivered to $Bbs10^{-/-}$ mice between ages of P23 and P31, when photoreceptor degeneration was at its initial stages. In each animal, one eye was treated, and the contralateral eye was left untreated as an internal comparison. Completely uninjected $Bbs10^{-/-}$ animals were also included in ERG studies to ensure that the ERG values of untreated eyes in treated animals were comparable with those of completely untreated animals.

Previously, we showed that the ERGs in $Bbs10^{-/-}$ mice become nonrecordable by 6–9 months of age.[14] To assess whether subretinal gene therapy maintains retinal function over time, ERG was performed at 1, 2, 3, 5, 9, and 10.5–12 months after treatment to measure the function of rods and cones in treated and untreated eyes.

To measure the rod function, eyes were subjected to 0.01 cd s/m^2 dim flash after overnight dark adaptation (DA) of the animals. For the 0.01 cd s/m^2 dim flash, a-wave amplitudes were small even in normal controls. Therefore, they are not illustrated. At 1.5 months post (MP) treatment, treated $Bbs10^{-/-}$ eyes had higher b-wave amplitudes compared with untreated eyes (Figures 3A and S5), suggesting that gene therapy can improve the function of the existing rod photoreceptors in treated retinas. In both treated and untreated eyes of $Bbs10^{-/-}$ mice, the b-wave amplitudes elicited by the 0.01 cd s/m^2 dim flash experienced a decline over several months, consistent with retinal degeneration. However, the decline in ERG amplitudes was slower in treated eyes compared with in untreated eyes, suggesting that gene augmentation slowed down the loss of rod photoreceptor function in treated eyes. At the experimental endpoint (10.5–12 MP treatment), the average b-wave magnitude of treated eyes was 52.032 ± 21.866 μV (n = 7), in contrast to 2.974 ± 0.718 μV in untreated eyes (n = 15). At the experimental endpoint, a notable ERG waveform was recorded in six of the seven treated eyes, while no ERG waveform

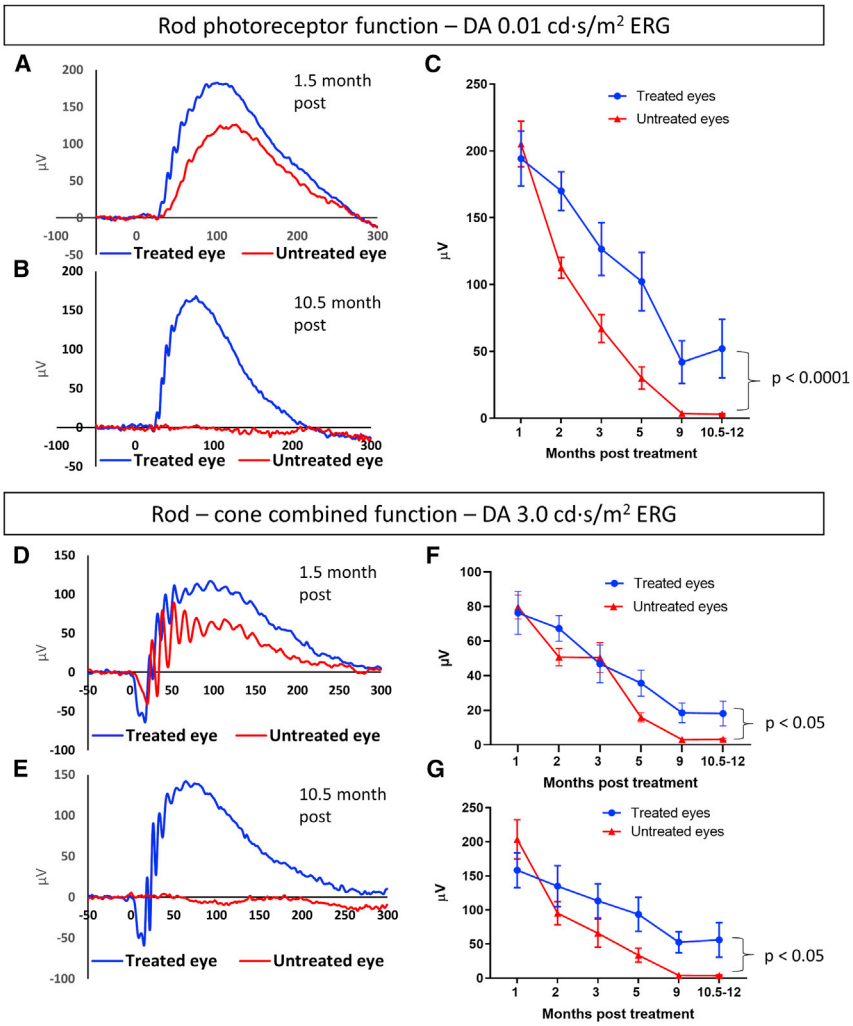

Figure 3. Subretinal gene therapy of BBS10 preserves significant rod and cone functions over the course of 10.5–12 months

(A–C) Rod function was measured by 0.01 cd s/m^2 dim flash after dark adaptation (DA). At 1.5 MP treatment, the treated eye had superior function compared with the untreated eye (A), and this response was sustained over 10.5 months, as the response in the untreated eye became non-recordable (B). Treated eyes had higher b-wave magnitudes compared with untreated eyes (C). (D–G) Combined rod-cone function was measured by 3.0 cd s/m^2 bright flash under dark-adapted conditions. At 1.5 MP treatment, the treated eye had a superior response (D), which was sustained over 10.5 months as the response in the untreated eye became non-recordable (E). Treated eyes had higher a- (F) and b- (G) wave amplitudes in combined response ERGs. Datapoints shown are averages ± standard error of the mean. p values of treatment effect using two-way ANOVA are shown.

was detected in any of the seven untreated contralateral eyes (Figure 3B). The treatment effect was statistically significant over the course of the experiment ($p < 0.0001$, two-way ANOVA, Figure 3C). These datasets suggest that subretinal gene augmentation therapy using AAV2/Anc80-*CMV-mBbs10* slowed down the loss of rod photoreceptor function in the retinas of *Bbs10*$^{-/-}$ mice.

Subretinal gene therapy slows the loss of rod and cone photoreceptor functions in treated eyes

The combined total function of rod and cone photoreceptors was measured by subjecting eyes to 3.0 cd s/m^2 bright flashes after DA of the animals (also known as standard combined response ERG). At 1.5 MP treatment, treated *Bbs10*$^{-/-}$ eyes had higher-amplitude responses to the stimuli compared with untreated eyes (Figures 3D and S5). In both treated and untreated eyes, the a-wave amplitudes declined over time, suggesting continued progression of degeneration at least in part of the retina. However, the observed decline was slower in treated eyes. In untreated eyes, the a-wave became essentially non-recordable by 9 MP treatment (Figure 3F). At the experimental endpoint (10.5–12 MP treatment), the average a-wave amplitudes of treated and untreated eyes were 18.12 ± 7.165 μV (n = 7) and 3.199 ± 0.559 μL (n = 15), respectively. The overall treatment effect was statistically significant ($p < 0.05$, two-way ANOVA; Figure 3G). The b-wave amplitudes of the standard combined response ERG, representing bipolar cell responses from both rods and cones, demonstrated a similar trend to the a-wave amplitudes. The decline of b-wave amplitudes in treated eyes was slower than that in untreated eyes (Figure 3G). At the experimental endpoint (10.5–12 MP treatment), the average b-wave amplitudes of treated and untreated eyes were 56.071 ± 25.250 μV (n = 7) and 3.803 ± 3.843 μL (n = 15), respectively. The overall treatment effect on ERG b-wave amplitudes was statistically significant ($p < 0.05$, two-way ANOVA; Figure 3G). At the endpoint, six of the seven treated mice had recordable waveforms in their treated eyes when subject to the 3.0 cd s/m^2 stimulus, whereas none of the untreated contralateral eyes had recordable waveforms.

Subretinal gene therapy of BBS10 restores cone electrical function

Although rods are mainly responsible for vision in low-light conditions, cones are responsible for daytime, color, and high-acuity vision in humans. *Bbs10*$^{-/-}$ mice have a congenital lack of cone electrical function prior to notable degeneration on two different cone-specific ERG measures.[14] More specifically, after light adaptation (LA) to bleach the responses from rods, animals were subjected to 15 flashes of 3.0 cd s/m^2 light followed by 5-Hz flickering light with the same light intensity. We used both of these ERG measures to evaluate cone electrical functions in treated and untreated *Bbs10*$^{-/-}$ eyes. A previous study has

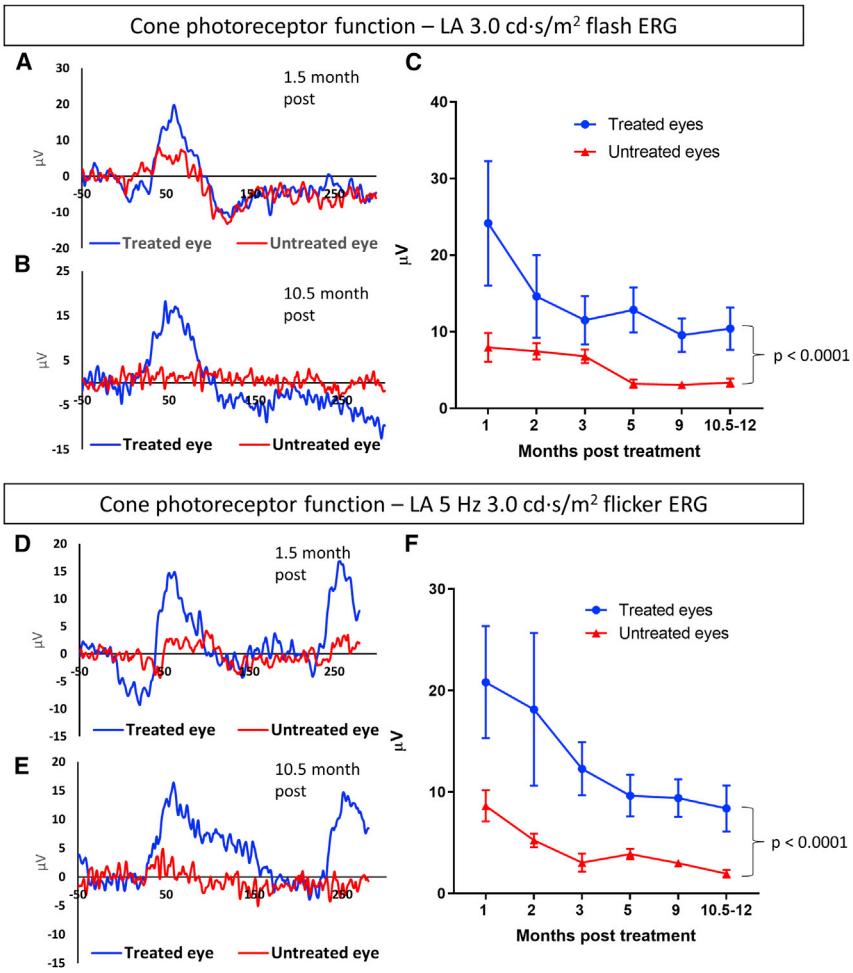

Figure 4. Subretinal gene therapy improves and sustains cone photoreceptor function in *Bbs10*$^{-/-}$ mice over the course of 10.5–12 months

Cone function was measured using two different assays after light adaptation (LA). (A–C) When subjected to a 3.0 cd s/m^2 bright flash, treated eyes had greater amplitudes compared with untreated eyes at 1.5 MP treatment (A) as well as 10.5 MP treatment (B). B-wave amplitudes of treated eyes were significantly better than those of untreated eyes (C). (D–F) When subjected to a 5-Hz flicker, cones in treated eyes elicited a periodic waveform at 1.5 months (D) and 10.5 MP treatment (E), which was not observed in the untreated contralateral eyes. Over the course of 10–11 months, treated eyes retained significantly better amplitudes in cone ERGs (F). Datapoints shown are averages ± standard error of the mean. p values of treatment effect using two-way ANOVA are shown.

shown that in *Cngα3*$^{-/-}$ mice, which lack cone photoreceptor function, there is an absence of recordable ERG signal at stimulus frequencies of 5 Hz and above. This result indicates that, at 5 Hz and above, the ERG responses are predominantly responses of the cone photoreceptor pathway.[20] The period of 10-min LA further reduced potential responses from rods. At 1.5 MP treatment, treated *Bbs10*$^{-/-}$ eyes had a robust response to the 3.0 cd s/m^2 bright flash, whereas untreated eyes continued to have a poor, stunted response to this stimulus (Figures 4A and S5). These data show that BBS10 gene therapy restores the electrical function in cones. We proceeded to determine whether the restoration of cone functions lasted in treated eyes. At the endpoint (10.5–12 months post treatment), treated eyes had higher b-wave amplitudes compared with untreated eyes (Figure 4C; treated eyes, 10.404 ± 2.742 μV, n = 7; untreated eyes, 3.372 ± 0.531 μV, n = 15). The stimulus light elicited a clear waveform in five out of the seven treated eyes, whereas untreated contralateral eyes displayed either barely or non-recordable responses (Figure 4B), suggesting that the regained cone electrical function was at least partly retained in most treated eyes over the course of the experiment (Figure 4C). The overall treatment effect was statistically significant ($p < 0.0001$, two-way ANOVA; Figure 4C). The 5-Hz flicker test, the second metric for measuring cone electrical function, showed outcomes similar to the first metric used. *Bbs10*$^{-/-}$ mice have a poor, stunted response to the 5-Hz flicker stimuli at all ages tested.[14] At 1.5 MP treatment, treated eyes demonstrated a clear periodic waveform in response to the 5-Hz flicker (Figure 4D). In contrast, the 5-Hz flicker stimuli never elicited a substantial response in their untreated contralateral eyes at any age (Figures 4D and 4E). At the experimental endpoint, treated eyes had greater responses to the 5-Hz flicker stimuli compared with untreated eyes, which lacked an identifiable waveform (treated eyes, 8.374 ± 2.271 μV, n = 7; untreated eyes, 1.950 ± 0.368 μV, n = 15; Figures 4E and 4F). At 10.5–12 MP treatment, four of the seven treated mice had a clear periodic waveform in their treated eyes, while no waveforms were observed in the untreated contralateral eyes. The overall treatment effect was statistically significant over the time course ($p < 0.0001$, two-way ANOVA; Figure 4F). Therefore, gene augmentation enabled cone photoreceptor cells to regain their electrical function in ERG, and in most cases the recovered cone function was retained or partially retained in the retina over 10–12 months.

Photoreceptors showed prolonged survival after gene augmentation therapy

To measure photoreceptor survival in the retina with and without gene augmentation therapy, OCT images were acquired to visualize the central retina as well as peripheral retinal regions. Under our experimental setting, viral vectors are delivered to the temporal region of the mouse peripheral retina. OCT images of the treated *Bbs10*$^{-/-}$ animal whose ERG traces are displayed in Figures 3A, 3B, 3D, and 3E, and Figures 4A, 4B, 4D and 4E, are shown in Figure 5A (treated animal 1). At 10 MP treatment, the treated eye of treated animal 1 had a readily visible layer of photoreceptor cells in optic-nerve-centered

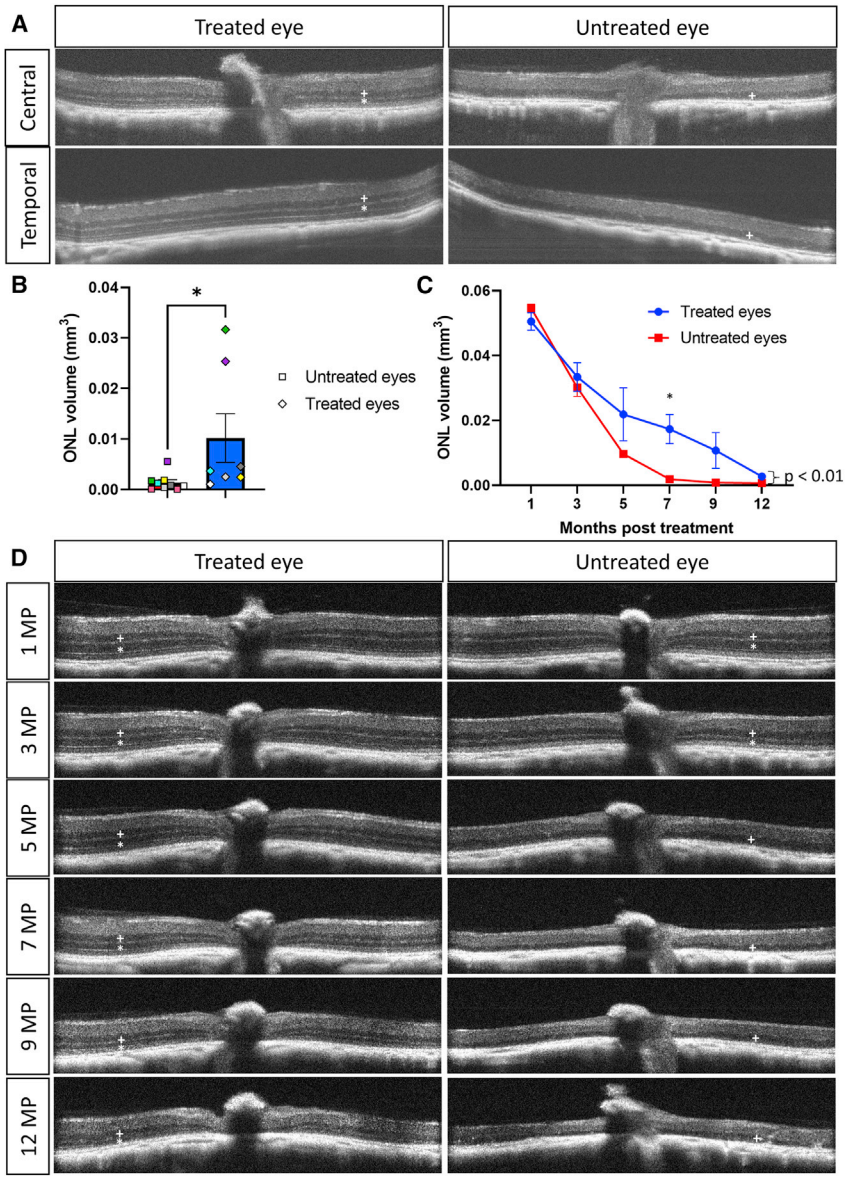

Figure 5. Gene therapy preserves photoreceptor survival over the course of at least 10 months

(A) OCT images centering on the optic nerve as well as visualizing the temporal region of the peripheral retina near the area of injection are shown for the treated and untreated contralateral eyes of treated *Bbs10*$^{-/-}$ animal 1. At 10 MP treatment, the photoreceptor layer ("*") is readily visible in the treated eye, but not in the untreated eye. The ONL is labeled with "*", and the INL is labeled with a "+" symbol. (B) ONL volume within OCT volumetric scans (with a diameter of 1,400 μm) was quantified in treated and untreated *Bbs10*$^{-/-}$ mice at 10–12 months post treatment. Datapoints of the treated and untreated eye pairs in an individual treated mouse are displayed as the same color. The error bar represents standard error of the mean, and statistical comparison was performed using one-tailed *t*-test. (C) OCT stacks were acquired for the treated and untreated eyes of 3 *Bbs10*$^{-/-}$ mice at 1, 3, 5, 7, 9, and 12 MP treatment and ONL volumes captured in the OCT stacks were quantified. Statistics shown to the right of the graph were acquired using two-way ANOVA, and statistics above individual datapoints represent those from Sidak's multiple comparisons. The error bar represents standard error of the mean. (D) OCT images for the treated and untreated eyes of a *Bbs10*$^{-/-}$ animal at 1, 3, 5, 7, 9, and 12 MP treatment are shown. The ONL is labeled with "*," and the INL is labeled with a "+" symbol.

OCT images as well as in images of the temporal region of the retina (Figure 5A, asterisk). In contrast, no ONL can be clearly discerned in OCT images of the untreated, contralateral eye of that animal (Figure 5A). We quantified the volume of the ONL within OCT volumetric scans of the retinas of seven treated and one untreated *Bbs10*$^{-/-}$ mice at 10–12 months after treatment. One OCT volumetric scan captures the retinal layers within a circular area of the retina with a diameter of 1,400 μm. ONL areas were manually segmented in consecutive serial images in an OCT stack and converted into volumes. Quantification of the ONL volume in OCT scans shows that gene augmentation partially preserved photoreceptors in treated eyes (Figure 5B). At 10–12 months after treatment, the average ONL volume in the OCTs of treated eyes was 0.0102 ± 0.0048 mm^3, and in untreated eyes was 0.0014 ± 0.0006 mm^3 ($p < 0.05$, one-tailed unpaired t test). In Figure 5B, datapoints of the treated and untreated eye pairs of each individual treated mouse are displayed in the same color. Datapoints of treated animal 1 are shown in purple; datapoints of treated animal 2 are shown in cyan. Gene augmentation preserved a group of photoreceptor cells in the retina over a significant portion of a mouse's adult life, when photoreceptors in the untreated eye have perished.

To determine whether gene augmentation therapy significantly slowed the rate of photoreceptor degeneration, we treated three *Bbs10*$^{-/-}$ mice in an OCT time course study and quantified the volume of the ONL in OCT volumetric scans of their treated and untreated eyes at 1, 3, 5, 7, 9, and 12 MP treatment (Figure 5C). These three animals received OCT scans at every time point. The datapoints of these three treated *Bbs10*$^{-/-}$ mice enrolled in the time course are colored in shades of gray in Figure 5B. In an untreated *Bbs10*$^{-/-}$ eye, the ONL degenerated over time and became difficult to observe in OCT by 7–9 MP treatment (Figure 5D). In contrast, the treated eye had a readily visible layer of ONL even at 12 MP treatment (Figure 5D). These data suggest that subretinal gene therapy delayed cell death and prolonged the survival of photoreceptors in treated eyes (Figure 5C; $n = 3$; $p < 0.01$, two-way ANOVA). However, photoreceptors in the treated eyes still

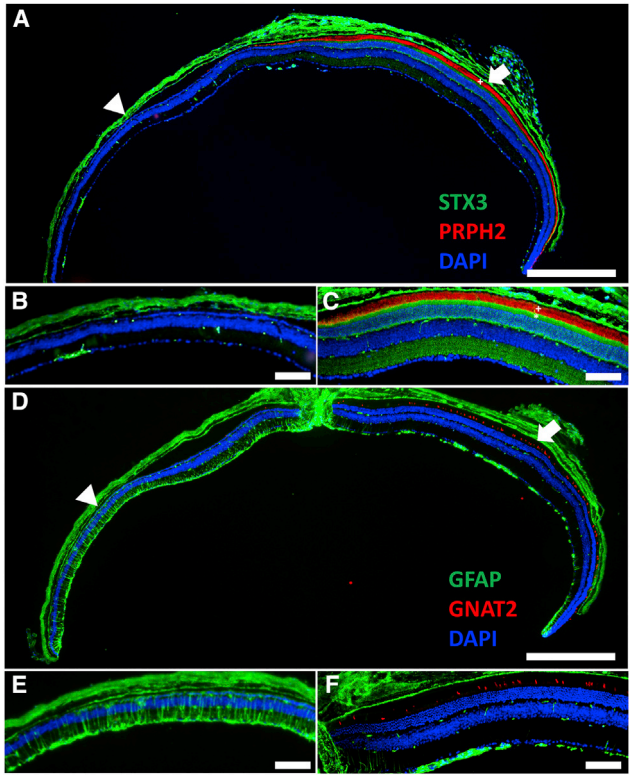

Figure 6. Rod and cone photoreceptors demonstrate long-term survival in the treated eye of treated animal 1 at 10.5 months post treatment

(A–C) At 10.5 MP treatment, a thick layer of photoreceptors, whose outer segments (marked with "+") are labeled with peripherin-2 (PRPH2), are readily observed in the treated region of the treated eye (A, arrow), but not in regions that were not transduced by the viral vector (A, arrowhead). In addition, STX3 localizes to the photoreceptor inner segments and synaptic layer, as expected, in the treated region of the treated eye (C), but not in untreated regions of the same eye (B). In (C), the outer segments are marked with "+," and the inner segments with "*." (D–F) Numerous cones, identified by cone-specific transducin subunit GNAT2, are observed in the treated region of the treated eye (D, arrow), but not in untreated regions (D, arrowhead, and E). Radially projected GFAP-positive filaments, indicative of activated Muller glia, span the untreated regions of the retina (D, arrowhead, and E), but are absent or nearly absent in the treated region of the same eye (D, arrow, and F). Scale bars, 500 μm in (A) and (D), and 100 μm in (B), (C), (E), and (F).

underwent a gradual, albeit slower, degeneration (Figure 5C). In this cohort of three treated *Bbs10*$^{-/-}$ animals, the ONL volume at 12 MP treatment was 0.00270 ± 0.00101 mm^3 in treated eyes, versus 0.00066 ± 0.00012 mm^3 in their untreated contralateral eyes (Figure 5C). Some treated *Bbs10*$^{-/-}$ animals, which were not part of this time course study, retained a much greater ONL volume in their treated eyes at the endpoint (Figure 5B). The cause behind this variability in efficacy is not completely understood and is a subject of further investigation. OCT experiments show that subretinal gene augmentation therapy using AAV2/Anc80-*CMV-mBbs10* delayed cell death and prolonged photoreceptor survival in an animal model of BBS10.

Rod and cone photoreceptors demonstrate long-term survival in treated Bbs10$^{-/-}$ animal 1

To identify rod and cone photoreceptors in treated and untreated eyes at the experimental endpoint, we performed immunohistochemistry to visualize rod and cone photoreceptor nuclei and outer segments in the retinas. In addition, we probed for the distribution of the BBSome cargo STX3, which showed outer segment localization in untreated *Bbs10*$^{-/-}$ retinas (Figure 1). We illustrate in detail the images from two treated *Bbs10*$^{-/-}$ animals (treated animals 1 and treated animal 2) and compare their treatment efficacy along with their respective ERG recordings.

In the treated eye of treated animal 1, a thick layer of photoreceptor nuclei (ONL) can be readily observed in addition to the inner nuclear layer (INL) in the treated region (Figure 6A, arrow), whereas only a single row of photoreceptor nuclei remains in untreated regions of the treated eye (Figure 6A, arrowhead). In the treated region, the outer segments of surviving photoreceptors are immunopositive for peripherin-2 (PRPH2), an outer segment marker (Figure 6A and 6C; photoreceptor outer segments are labeled with "+"). In addition, STX3 localizes to the inner segments of these surviving photoreceptor cells (Figure 6C; photoreceptor inner segments are labeled with "*") as well as to the outer plexiform layer, as in normal photoreceptors. These data indicate that a group of photoreceptors survived for more than 10 months after treatment and maintained normal distribution of the BBSome cargo, STX3. This observation suggests that the BBSome function was at least partially restored in the treated photoreceptor cells. The ERG recordings of this animal are displayed in Figures 3A, 3B, 3D, 3E and Figures 4A, 4B, 4D, 4E.

In ERG experiments, the gene therapy treatment improved the electrical functions of cones in the retinas, which were sustained or partially sustained over the course of 10–12 months. Therefore, we probed the retinal sections with an antibody against G-protein subunit α transducin 2 (GNAT2), a cone-specific protein, to identify the presence of cone outer segments. In the treated eye of animal 1, numerous GNAT2-positive cone outer segments are observed in the treated region (Figure 6D, arrow, and Figure 6F), indicating the presence of surviving cones. Few or no cones are observed in the untreated regions of the injected eye (Figure 6D, arrowhead, and 6E) or in the uninjected contralateral eye (Figure S6), suggesting that cones that were not transduced by the gene therapy vector have largely perished at 10.5 MP treatment.

In addition, we looked for markers of active retinal degeneration in treated and untreated eyes. Active retinal degeneration is typically accompanied by the presence of inflammatory markers in Muller glia, including glial fibrillary acidic protein (GFAP). Muller glia, processes of which encompass the ganglionic layer to the outer limiting membrane, are normally devoid of detectable GFAP expression in healthy physiological conditions.[21] Retinal astrocytes, on the other hand, are normally GFAP positive, and are restricted to the retinal nerve fiber layer.[21] In response to experimental injuries or a genetic condition with photoreceptor degeneration, GFAP becomes expressed

in retinal Muller glia, and GFAP+, radially oriented processes across the retina can be observed.[21] Therefore, we probed the retinas with an anti-GFAP antibody in addition to GNAT2. When we looked for these indications of active retinal degeneration, the treated area of the injected eye notably lacks radially oriented GFAP+ processes (Figure 6D, arrow, and Figure 6F), whereas numerous such processes are observed in the untreated regions in the same eye (Figure 6D, arrowhead, and Figure 6E). Radial GFAP+ processes are also abundant in the untreated contralateral eye (Figure S6). Together, these data suggest that a pool of photoreceptors survived until the endpoint in the treated eye. In addition, the treated region in the treated eye had substantially lower levels of markers of active degeneration, suggesting that retinal degeneration is drastically reduced by gene augmentation therapy.

Photoreceptor survival and electrical functions of treated Bbs10$^{-/-}$ animal 2

At 10.5 MP treatment, retinas of treated animal 2 were probed with anti-STX3 and anti-RHO antibodies. Similarly, in the treated eye of animal 2, there is a region containing a pool of photoreceptors at 10.5 MP treatment (Figure 7A, arrow, Figure 7C), although the treated region of this animal appears to be smaller than that in the treated eye of treated animal 1. Within the treated region (Figure 7A, arrow), the photoreceptor outer segments are immunopositive for PRPH2 (Figure 7C; outer segments are marked with "+"), and STX3 localizes to photoreceptor inner segments (Figure 7C; inner segments are marked with "*"). A group of photoreceptors survived until 10.5 MP treatment in the treated eye of treated animal 2.

To gain insight into whether the size of treated regions affects the treatment efficacy, we compared the histological and functional data of treated animals 1 and 2. In terms of the ONL endpoint volumes, treated animal 2 had the median value of the seven treated mice, whereas treated animal 1 had the second highest ONL volume of the group (Figure 5B). The ERG recordings of treated animal 2 at 1.5 MP, 8.5 MP, and 10.5 MP treatment are shown in Figures 7D–7F. In the treated eye of animal 2, the ERG amplitudes in response to the 0.01 cd s/m^2 dim flash declined from 1.5 MP (Figure 7D) to 8.5 MP treatment (Figure 7E). However, the amplitude was largely maintained between 8.5 MP and 10.5 MP treatment (Figures 7E and 7F), suggesting that degeneration of the survived photoreceptors was drastically slowed. In contrast to rods, amplitudes of ERG metrics measuring cone function (the light-adapted 3.0 cd s/m^2 single flash and the 5-Hz flicker) did not decrease between 1.5 and 10.5 MP (Figures 7D and 7F). A potential explanation is that, while untreated cones perished over time, the treatment caused a substantial gain of function in treated cones. Since ERG recordings capture the sum of the electrical functions throughout the retina, the occurrence of these two events (the loss of some cones and the gain of function of treated cones) causes the overall amplitude to be comparable over time. The presence of surviving photoreceptors in the treated eye of animal 2 is consistent with the robust recordings of rod and cone electrical functions at the endpoint of the experiment (Figure 7F).

Functional daytime vision is preserved by BBS10 subretinal gene therapy

To determine whether gene therapy conferred a benefit in functional vision, we tested the functional vision of mice with the visually guided swim assay, which is a quantitative measure of rodent vision. This test can be performed under different lighting conditions to evaluate rod- and cone-dependent visual pathways. In this assay, a mouse, placed inside a pool, is trained to visually identify and swim to a platform. For 20 different trials, the platform is randomly placed inside the pool in each trial to prevent memorization by the rodent. The average time it takes for a mouse to reach the platform (time to platform) provides a quantitative measure of the rodent's functional vision. Similar to the multi-luminance mobility test used in human clinical trials, the visually guided swim assay can be used to determine functional vision at different lighting levels. We conducted vision testing under two different lighting conditions: first, in a room lit by normal fluorescent ceiling light measuring 13.35 cd/m^2 (light condition) as well as in a dark room with only dim red lighting measuring 4.17×10^{-3} cd/m^2 (dark condition). Under the light condition, vision is predominantly supported by the cone pathway, whereas, under the dark condition, vision is predominantly provided by the rod pathway. We have previously shown that wild-type or heterozygous control mice have an average time to platform of around 3–5 s in both light and dark conditions, and that their average time to platform remains stable over their lives.[14] In contrast, we have shown that *Bbs10*$^{-/-}$ mice have worse vision than normal controls at 6 months of age in both light and dark conditions, and that this swim assay is sensitive enough to detect differences in the rates of visual decline between the *Bbs10*$^{-/-}$ mutants and *Bbs1*$^{M390R/M390R}$ mutants, with *Bbs10*$^{-/-}$ being more severe.[14]

To determine whether subretinal gene therapy prevents the loss of vision in BBS, mice that received gene therapy treatment (in one eye only) and untreated *Bbs10*$^{-/-}$ mice were tested at 4–6 months of age (3–5 months after treatment) and then at 9–12 months of age (8–11 months after treatment) in both light and dark conditions. Injected or uninjected wild-type and heterozygous mice were also included to ensure reproducibility of the assay. For wild-type or heterozygous mice, their time to platform in the light was 3.05 ± 0.94 s (n = 2) between 4 and 6 months of age, and 3.13 ± 0.28 s (n = 4) between 9 and 12 months of age (Figure 8), exhibiting stable vision over time as previously described.[14] In contrast, untreated *Bbs10*$^{-/-}$ mice had an averaged time to platform of 11.48 ± 3.25 s in the light between 4 and 6 months of age, which worsened to 28.34 ± 1.59 s between 9 and 12 months of age, consistent with a gradual loss of vision due to retinal degeneration (Figure 8). On the other hand, treated *Bbs10*$^{-/-}$ mice had an averaged time to platform of 7.13 ± 1.37 s in the light between 4 and 6 months of age, and 12.25 ± 3.40 s between 9 and 12 months of age, requiring 38% and 57% less time to complete this visual task than their untreated counterparts at these ages (Figure 8). The data suggest that treated *Bbs10*$^{-/-}$ mice see significantly better than their untreated counterparts in the light at 8–11 months after therapy and that BBS10 gene therapy provided long-lasting benefits in preserving functional daytime vision in treated mice.

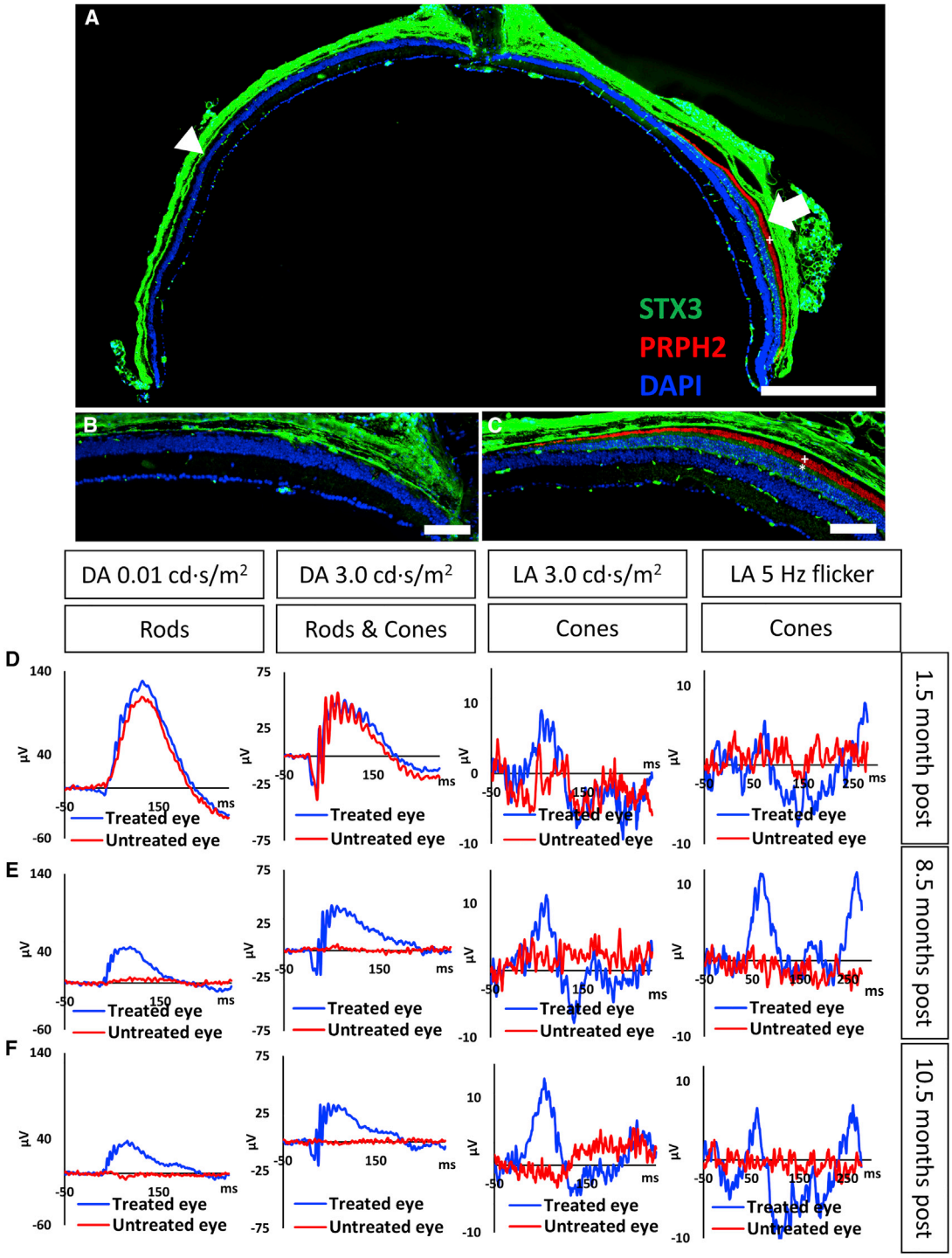

Figure 7. Photoreceptors demonstrate long-term survival in the treated eye of *Bbs10*$^{-/-}$ animal 2 at 10.5 months post treatment

(A–C) In the treated eye of treated *Bbs10*$^{-/-}$ animal 2, photoreceptors, whose outer segments (marked with "+") are labeled with peripherin-2 (PRPH2), are readily observed in the treated region of the eye (A, arrow), but not in untreated regions (A, arrowhead, and B). In addition, in the treated region, STX3 localizes to the photoreceptor inner segments and synaptic layer, as expected (C), but not in untreated regions of the same eye (B). In (C), the outer segments are indicated with "+," and the inner segments with "*." (D–F) ERG recordings of this treated *Bbs10*$^{-/-}$ animal at 1.5 (D), 8.5 (E), and 10.5 MP treatment (F) are shown. Clear waveforms were recorded at the endpoint in both rod- and cone-specific measures in the treated eye, but not in the untreated contralateral eye (F). Scale bars, 500 μm in (A), and 100 μm in (B) and (C).

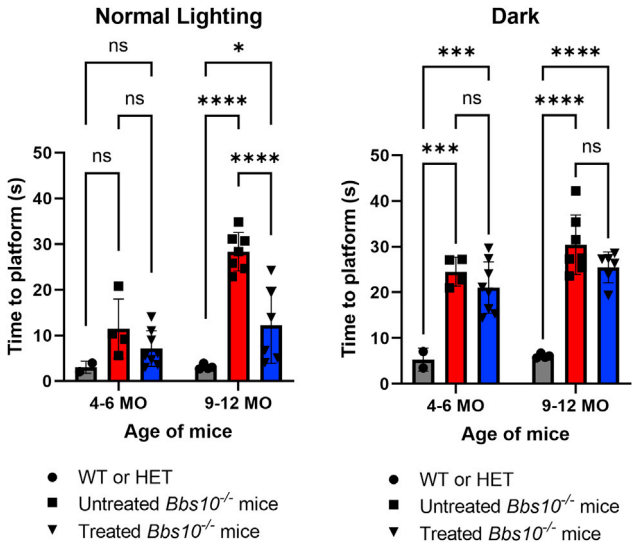

Figure 8. Subretinal gene therapy prevents or delays the loss of functional vision in light and dark testing conditions

In normal room lighting, *Bbs10*$^{-/-}$ mice treated with subretinal gene therapy took significantly less time to locate the platform compared with their untreated counterparts at 9–12 months of age. Subretinal gene therapy also provided a minor benefit to treated mice when navigating in dark conditions compared with untreated *Bbs10*$^{-/-}$ mice. Each datapoint represents the averaged swim time of a mouse, and the error bar represents the standard error of the mean. Statistical comparisons were made using two-way ANOVA followed by Sidak's multiple comparisons test.

To determine the effect of subretinal gene therapy on vision in low-light conditions, mediated by rods, the visually guided swim assay was performed in these mice under "dark-swim" conditions. The assay was conducted in a dark room facilitated by dim red lighting (see section "materials and methods"). For untreated *Bbs10*$^{-/-}$ mice, the averaged time to platform in the dark was 24.53 ± 1.58 s between 4 and 6 months of age, which worsened to 30.43 ± 2.46 s between 9 and 12 months of age, consistent with the gradual loss of night vision due to degeneration of rod photoreceptor cells (Figure 8). On the other hand, for *Bbs10*$^{-/-}$ mice that received subretinal gene therapy, the averaged time to platform in the dark was 21.06 ± 2.00 s between 4 and 6 months of age, and 25.48 ± 1.38 s between 9 and 12 months of age, requiring 14% and 16% less time than their untreated counterparts to find the platform at these ages (Figure 8). These results support the notion that subretinal gene therapy provided a small benefit in preventing the loss of low-light vision over the BBS disease course.

In summary, subretinal gene augmentation by AAV2/Anc80-*CMV-mBbs10* prolonged the survival of rod and cone photoreceptors in treated retinas and maintained or partially maintained retinal functions of treated eyes for at least 10–12 months. Considering the lifespan of laboratory mice, intervention by subretinal gene therapy provided tangible benefits in cell survival and in functional vision persisting over a significant portion of a mouse's adult life. Notably, subretinal gene augmentation therapy partially restored the electrical function of existing cone cells in *Bbs10*$^{-/-}$ mice, and these restored functions were maintained fully or partly in the majority of the treated mice for 10–12 months.

DISCUSSION

Subretinal gene therapy for BBS10 shows long-term efficacy and delayed degeneration

Mutations in *BBS10* account for more than a fifth of all BBS cases. Gene therapy development for BBS10 holds immense promise for improving the health and quality of life for these patients. In the current study, we tested subretinal gene augmentation therapy by treating 23-31-day-old *Bbs10*$^{-/-}$ animals and followed the animals for up to 10–12 months after treatment to evaluate long-term efficacy. Long-term therapeutic efficacy was evaluated using multiple experimental modalities, including ERG, OCT, histology, and a functional vision assay. Together, these experiments provided evidence that subretinal gene therapy using AAV2/Anc80-*CMV-mBbs10* substantially delayed photoreceptor degeneration, restored electrical functions of cone photoreceptors, and partially preserved functional vision in treated mice. These therapeutic effects were evaluated up to and persisted for a period of 10–12 months, lasting throughout a significant portion of the lifespan of laboratory mice. Volumetric quantification of the ONL using non-invasive OCT imaging in the same cohort of mice over time showed that photoreceptors in the treated regions had a slower rate of loss compared with photoreceptors in corresponding regions in untreated contralateral eyes. ERG analysis showed that retinal electrical function remained recordable in the majority of treated eyes until 10–12 MP treatment when the electrical functions in their untreated contralateral eyes became non-recordable. Immunohistochemistry revealed the presence of rods and cones in treated eyes with outer segments and physiologically normal distribution of BBSome cargo, STX3, indicating that BBS10 enabled the BBSome to carry out cargo transport functions in treated cells. Restored cargo distribution likely contributes to the slowing of photoreceptor cell death, as protein mislocalization between the inner and outer segments causes cellular stress and photoreceptor degeneration.[4] Visually guided swim assay showed that treated mice had superior functional vision in the light and dark, even at 9–12 months of age. These pieces of evidence support the conclusion that subretinal gene augmentation therapy for BBS10 significantly delays vision loss in a BBS10 animal model.

Subretinal gene augmentation therapy enables the recovery of cone electrical function

Notably, subretinal gene augmentation not only preserved but increased the function of treated cones in the retina. Cone photoreceptors in *Bbs10*$^{-/-}$ mice have congenitally low or nearly absent electrical function in ERG prior to substantial retinal degeneration.[14] Subretinal delivery of the viral vector encoding BBS10 enabled the recovery of robust cone-specific electrical signals in two different ERG tests. Cones with outer segments survived for at least 10–12 months, visualized by immunohistochemistry. We

then investigated whether the presence of these cones and their electrical activity were accompanied by a functional benefit in vision.

BBS10 gene therapy preserves functional vision in a mouse model of BBS10

The presence of a recordable ERG signal does not directly correlate with the presence of functional vision. The most direct measure of therapeutic efficacy is functional vision. Conducted at 4–6 months of age and then again at 9–12 months of age, these experiments showed that gene therapy significantly delayed the complete loss of vision in these mice. Even when injected only unilaterally, treated *Bbs10*$^{-/-}$ mice took 57% and 16% less time than untreated *Bbs10*$^{-/-}$ mice to complete visual tasks in the light and in the dark at 9–12 months of age. Overall, a robust preservation of day vision was observed in mice treated with subretinal gene therapy, which was accompanied by the survival of cones and the presence of cone electrical activities, suggesting that gene augmentation therapy can significantly delay vision loss in BBS10.

Treatment efficacy correlates with the apparent size of the treated region

In this study, we noted an apparent correlation between the size of the treated area and the ERG amplitudes observed in the animal. Depending on the injection, the size of the raised subretinal bleb and therefore the size of the region treated by the vector may vary from animal to animal. In other words, the injected viral vector does not reach the entire area of the retina, but only the regions around the site of injection. In our experiments, the size of this region partly accounts for the variability observed in gene therapy efficacy. In this study, we noted the potential effect of the size of the treated region on treatment efficacy at the functional level. The smaller apparent treated region in the treated eye of animal 2 compared with animal 1 corresponds to the smaller ERG amplitudes recorded at the endpoint in treated animal 2 compared with in animal 1. A plausible explanation is that more photoreceptor cells were lost in treated animal 2 over time given the smaller treated region. However, regardless of the size of the treated region, the surviving photoreceptors in both animals seemed to show perdurance. The correlation of greater treated area and more surviving photoreceptors with higher ERG amplitudes in animal 1, and the proportionally lower, though robust, numbers of photoreceptors and ERG amplitudes in animal 2, supports a connection between anatomic and functional rescue. More experiments are needed to verify this observation.

Additional challenges in gene therapy remain to be addressed

Previously, to test the feasibility of gene therapy for BBS, we developed a *Bbs8* mouse line in which *Bbs8* gene expression, initially inhibited by a gene trap placed within the gene, can be re-activated at any age. Injection of *Bbs8*$^{gt/gt}$; *Flp*$^{+}$ mice (mice homozygous for the inhibitory gene trap insertion in the *Bbs8* gene) with tamoxifen induces the expression of tamoxifen-inducible *Flp* recombinase, which removes the gene trap and enables the assembly of the complete BBSome under precise temporal control. Restoring BBSome function in immature retinas by tamoxifen injections between P9 and P15 mimics the effect of early gene augmentation. Early gene augmentation fully ameliorated retinal phenotypes in *Bbs8*$^{gt/gt}$; *Flp*$^{+}$ mice.[5] After removal of the gene trap and re-activation of *Bbs8*, malformed photoreceptor outer segments were replaced by new, properly stacked outer segments in *Bbs8*$^{gt/gt}$; *Flp*$^{+}$ mice. STX3 mislocalized to the outer segments of *Bbs8*$^{gt/gt}$; *Flp*$^{+}$ mice was cleared along with the malformed outer segments, and the retinal phenotypes of treated mice were closely comparable with that of normal controls.[5] This study demonstrated that early gene augmentation is feasible.

However, the delivery of a BBS gene by vehicles such as AAV is more challenging. For example, the overexpression of exogenous *BBS1* gene caused toxicity in retinal cells, speaking to the importance of gene dose.[22,23] Target gene expression can be additionally influenced by the choice of AAV as well as the choice of promoters to drive expression.

After transduction by AAV, the transgene remains in the host cell as episomal DNA. Even when adequate transduction and expression are achieved initially, whether the delivered transgene maintains lasting expression over time is complicated by additional factors. In non-dividing cells such as in terminally differentiated photoreceptors, even though the transgene would not be diluted by cellular division, various mechanisms can still negatively influence gene expression. For example, both the viral capsid and the foreign episomal DNA can induce an immune response, leading to the potential destruction of the host cell. Moreover, the promoter of the transgene can become silenced by epigenetic modifications. These factors, among others, can lead to the reduction of transgene expression over time, resulting in the attenuation of therapeutic effect. Additionally, treated photoreceptors can be negatively affected by the degeneration of the surrounding untreated photoreceptors. If the gene dose was insufficient, BBSome function may have been partially but not fully restored in treated cells. The reason why photoreceptor cells in treated eyes still experienced a slowed but gradual cell death despite *Bbs10* gene augmentation is unknown. Addressing the cause(s) behind the attenuation of long-term therapeutic efficacy is an area of active research.

AAV2/Anc80 is a potent vehicle for treating BBS10 with subretinal gene therapy

Blindness in BBS is caused by photoreceptor cell death. Therefore, the delivery of the transgene to photoreceptors has been the primary focus of gene delivery in BBS. Nevertheless, emerging evidence involves the RPE,[24] inner retinal neurons,[25] and endothelial cells[26] in BBS pathologies in the retina. Shown by RNA sequencing, RPE lacking *Bbs8* has a marked downregulation of adult-RPE-specific genes and an upregulation of fetal RPE-specific genes in 1-month-old mice, suggesting that *Bbs8*-deficient RPE has delayed maturation.[24] At the functional level, cultured RPE cells lacking BBS8 have a reduced ability to phagocytose photoreceptor outer segments,[24] one of their principal functions in maintaining physiologic retinal homeostasis. Traditionally thought to solely affect photoreceptor cells, a more complete picture is emerging in which BBS genes play a role

in the function of various retinal cell types. Further research investigating the necessary cellular targets for gene therapy will be important for therapy design.

For the purpose of enhancing cellular transduction profiles, the AAV2/Anc80 viral vector was engineered using ancestral sequence reconstruction techniques. This AAV2/Anc80 capsid is the predicted common ancestor of most known primate AAVs that are currently used for gene therapy applications, including serotypes 1–3 and 6–9.[27] During the development of this viral capsid vehicle, multiple Anc80 variants were tested, each exhibiting a somewhat different cellular tropism.[27] This AAV2/Anc80 vector, the L65 variant subtype in this case, was shown to be highly tropic for retinal photoreceptors and RPE when injected subretinally.[19] Using AAV2/Anc80-*CMV-GFP*, we were able to validate and replicate this observation in our study. In addition, transduction of some Muller glia and ganglion cells was also noted after subretinal delivery.[19] We also observed GFP expression in inner retinal cells. Since we cannot rule out the importance of non-photoreceptor cells in achieving optimal gene therapy efficacy, a viral vector with a broad-targeting profile is ideal for gene delivery.

Advancing a novel viral vector to clinical use requires extensive testing; it is therefore worthwhile to explore other AAVs with similar cellular tropism. Using an eGFP transgene packaged into the viral constructs, AAV2/Anc80 and AAV8 showed a similar transduction profile in the retina following subretinal delivery, although a higher level of expression per photoreceptor was consistently achieved with the AAV2/Anc80 viral vector.[19] Importantly, cone photoreceptors were transduced as well as rods after subretinal delivery of a total dose of 2×10^9 genome capsids in mice (in 2 μL). The AAV2/Anc80 L65 viral capsid transduced 66% of cones in the mouse retina after subretinal delivery, compared with 41% by AAV8 under similar experimental settings.[27] GFP expression in both cones and rods was also observed in rhesus monkeys subretinally treated with this vector at the dose of 1×10^{10} total genome capsids delivered in 150 μL.[27] Since rods, cones, and RPE are known to be affected in BBS, the AAV2/Anc80 viral vector or a vector with a similar tropism is well suited for treating retinal degeneration in this disorder. Indeed, in our study, a robust rescue in cone photoreceptor function was observed after treatment, and cone-mediated daytime vision was preserved. Whether the transduction of the RPE was an essential component of the observed efficacy is unknown and merits investigation.

Gene therapy outcomes for different BBS genes depend on their gene function

Another successful instance of gene augmentation therapy for BBS was demonstrated for BBS4, which is a component of the BBSome. Using an AAV containing the mouse *Bbs4* gene driven by the mouse opsin promoter, *Bbs4*$^{-/-}$ mice were treated at 2 weeks of age, and the survival of retinal photoreceptors was evaluated in 12- to 16-week-old animals and in one 45-week-old animal (about 10 months after treatment). At 10 months after treatment, the treated *Bbs4*$^{-/-}$ animal had six or seven rows of photoreceptor nuclei around the injection site in the treated eye, whereas the untreated eye was devoid of photoreceptors at that age.[28] The mouse opsin promoter used would limit the expression of *Bbs4* to photoreceptor cells. It is not clear whether efficacy would be even higher if the expression of *Bbs4* was not limited to photoreceptors by using a photoreceptor-specific promoter to drive expression. This study shows that retinal degeneration in *Bbs4*$^{-/-}$ mice can be treated by the exogenous delivery of the *Bbs4* gene.

It is not clear whether mutations in any BBS gene can be treatable by gene augmentation using a similar approach. Feasibility of gene therapy in another BBS gene, the Leucine zipper transcription factor like 1 (*Lztfl1*), was investigated using a *Lztfl1* mouse model with a removable gene trap construct similar to that used for *Bbs8*. *Lztfl1* directly interacts with the BBSome through BBSome component BBS9, and acts as a negative regulator of the ciliary localization of the BBSome.[29] Mimicking gene augmentation of *Lztfl1* by tamoxifen-induced removal of the inhibitory gene trap was found to delay photoreceptor degeneration in treated mice but did not achieve complete phenotypic rescue, unlike that observed in the *Bbs8* model. Specifically, removal of the gene trap inhibiting *Lztfl1* by tamoxifen treatment at P5, P8, and P12 largely restored photoreceptor outer segment morphology, but did not correct mislocalization of STX3 to the outer segments.[30] Even in newly formed outer segments (at 3 months after tamoxifen treatment), the majority of STX3 still mislocalized to the photoreceptor outer segments, in contrast to the results observed in the *Bbs8* mouse model. These results suggest that *Lztfl1* may play a role in ciliary structural formation in addition to acting as the negative regulator of the ciliary localization of the BBSome, and the lack of this role during ciliary formation cannot be amended by treatment at a later stage. The time window amenable to gene augmentation therapy for another BBS gene may depend on the role of that particular gene. As a result, there may not be a globally applicable rescue time window in BBS due to the heterogeneity of gene functions. Patients with *BBS10* mutations appear to have more severe retinal degeneration than patients with *BBS1* mutations.[17] Visual acuity declined more rapidly in patients with *BBS10* mutations compared with those with *BBS1* mutations.[17] In BBS mouse models, genuine differences in rates of degeneration were also observed.[31,32] Mechanistic knowledge of gene function is a key element in the optimal design of gene therapy.

Additional tasks lay ahead for the clinical translation of BBS10 subretinal gene therapy

Many tasks lay ahead for the translation of a therapy from small animals to the clinics. The optimization of the DNA expression cassette and viral capsid to minimize immunogenicity, the gathering of additional data on safety and toxicity profiles of the vector, dose translation from small laboratory animals to humans, understanding the time windows amenable to gene augmentation, establishing appropriate recruitment criteria of patients, and selection of relevant endpoints for the evaluation of therapeutic efficacy are only a few examples of the myriad of design considerations.

Dose scaling from mice to larger species is not a straightforward task, but lessons can be learned from past examples of successful gene therapy development. To develop treatments for RPE65-associated Leber congenital amaurosis (LCA), a mouse model, *rd12*, was successfully treated using the rAAV5-CBA-h*RPE65* vector delivered at 1×10^{10} particles in 1 μL.[33,34] In another study in which AAV2.*RPE65* was delivered subretinally to both mice and dogs to treat LCA, a total dose of 1×10^{9} was delivered in mice (in 1–3 μL),[35] whereas a total dose of 8.25×10^{10} vg was delivered in 150 μL in dogs (with a concentration of 5.5×10^{8} vg/μL).[36] In that particular study, dose escalation from mice to dogs entailed an 82.5-fold increase in total dosage. This therapy was developed into a successful clinical therapy for humans. Using voretigene neparvovec (AAV2-h*RPE65*v2), a total dose of 1.5×10^{11} vg was injected per eye in a volume of 300 μL into patients with LCA (in a concentration of 5×10^{8} vg/μL).[37] The total dosage for treating humans (using a similar vector) represented a 150-fold increase in dose used in mice. In this case, the concentration of the vector used remained in a similar range for mice, dogs, and humans, and the escalation of total dose was mainly a function of the increase in injection volume. These past examples can serve as initial guidelines for dose scaling. Additional factors may come into play, including, but not limited to, difference in the sizes of treated areas in mouse and humans, total number of treated cells, and variability in photoreceptor density between species. On average, the mouse retina has approximately 500,000 photoreceptors per square millimeter.[38] In contrast, human retina has approximately 140,000 photoreceptor per square millimeter.[38] Dose scaling may therefore take into consideration the total number of treated cells based on bleb volume and cell density. Studying larger animal models such as dogs or non-human primates may provide useful insights. Notably, a non-human primate model of BBS7 has been found, which occurred naturally in a colony of rhesus macaques.[39] Strategies for effective interspecies dose scaling are an important area of translational research. The human eye reaches 90% of adult size at approximately 2 years of age. Before 2 years, injection volume requires adjustment, adding another layer of consideration.

An important aspect of this study was the identification of appropriate endpoints for evaluating therapeutic efficacy, and the endpoints chosen for this study mimicked those selected for human clinical trials of different retinal dystrophies. For example, for treating patients with LCA caused by *RPE65*, the multi-luminance mobility test, a quantitative measure of vision, was chosen as the primary endpoint.[37] This test measures the ability of the patients to navigate a 5-foot by 10-foot course with obstacles in or adjacent to the course. In this current study, the rodent visually guided swim assay provided a quantitative measure of vision, and can be similarly performed at different lighting levels. In addition, we demonstrated the utility of using ONL volume in volumetric OCTs of the retina as a secondary endpoint to assess the degree of photoreceptor degeneration. Comparing ONL volume in treated and untreated eyes over time can help determine whether the treatment altered the rate of degeneration. Measurement of the width of the ellipsoid zone (EZ) in OCT has been suggested for human studies.[40] However, some patients lose the EZ line early in the course of their disease.

Although many open questions remain, we demonstrated that subretinal gene therapy in a mouse model of BBS10 can delay vision loss in BBS. Addressing challenges in the attenuation of long-term efficacy, determining the viability of late-stage treatment, furthering the understanding of dose-response and interspecies dose translation, and taking initial steps toward clinical translation are among the top priorities at present.

MATERIALS AND METHODS

Study design

In this study, the long-term efficacy of subretinal gene therapy was evaluated in a preclinical mouse model of BBS10. *Bbs10*$^{-/-}$ animals between P23 and P31 received subretinal injections of the gene therapy vector containing the *Bbs10* gene (AAV2/Anc80-*CMV-mBbs10*). In these treated animals, only one eye received the subretinal gene therapy treatment, and the contralateral eye served as the untreated control. Completely untreated *Bbs10*$^{-/-}$ mice were also included in ERG and OCT experiments. To evaluate the effect of the subretinal injection procedure on the retina, sham injections delivering the injection buffer only was performed in heterozygous or wild-type animals and they were compared with untreated heterozygous or wild-type animals. Both male and female mice were used in this study. Outcome measures include ERG, OCT, immunohistochemistry, and visually guided swim assay. ERG was performed at 1, 2, 3, 5, 7, 9, and 11 MP treatment, and OCT was performed at 1, 3, 5, 7, 9, and 12 MP treatment, to evaluate retinal function and photoreceptor survival over time.

Exclusion criteria

The subretinal injection procedure creates a temporary separation of the retina from the RPE, a subretinal bleb, where a part of the retina is elevated and separated from the RPE to accommodate the injected fluid. The success of the subretinal injection can be determined by the presence of the subretinal bleb immediate after the injection. At the time of the subretinal injections, the size of the retinal blebs was visually assessed for each animal under the Zeiss OPMI f 170 surgical microscope, and those animals that had small or no retinal blebs immediately after the injection were excluded from the study. Cases with retinal detachment that did not resolve after injection were also excluded.

An exclusion criterium was established for the visually guided swim assay. In rare instances, mice that had no desire to swim and repeatedly floated in the pool during experimentation were encountered. All data from a mouse (light and dark testing) was discarded if the mean swim time of a mouse was greater than 1 standard deviation from the median of the group, and, consistent floating (floating more than three times per test episode or more than three corrections of floating per test episode, either by snapping fingers to create an audible sound or by flicking of the mouse's tail) was also present.

Table 1. Primers for *Bbs10* genotyping

Primer	Ratio (%)	Sequence (5′ to 3′)
Bbs10KO-WT-Fr	20	CCCATGGTAAGTGGTCAATCAG
Bbs10KO-MT-Fr	45	TCAATGTATCTTATCATGTCTG
Bbs10KO-WT-Rv	35	TGGTCTGGTGGACTCAATGGAC

Human patient

The retrospective review of human OCT data was approved under IRB# 202002294 by the Institutional Review Board at the University of Iowa. OCT scans were obtained using the Heidelberg OCT (Franklin, MA) or Zeiss Cirrus OCT at the University of Iowa. Quantification of ONL thicknesses was performed using ImageJ at a distance 2000 μm from the fovea. Full-field ERGs were obtained using the Diagnosys system using the standard International Society for Clinical Electrophysiology of Vision (ISCEV) protocols as previously described.[41]

Animal husbandry and ethics statement

This study was performed in strict accordance with the recommendations in the Guide for the Care and Use of Laboratory Animals of the National Institutes of Health. All the animals were handled according to approved Institutional Animal Care and Use Committee (IACUC) protocol #1041421 of the University of Iowa. The *Bbs10* mouse model was acquired from the KOMP2 Center at the Jackson Laboratory, and it is now distributed through the Mutant Mouse Resource and Research Centers (MMRRC) as C57BL/6N-*Bbs10*$^{tm1.1(KOMP)Vlcg}$/JMmucd. This mouse model was generated from the embryonic stem (ES) cell line *Bbs10*$^{tm1(KOMP)Vlcg}$ (VG13389A-A11, MMRRC). The C57BL6/NJ congenic version of the *Sox2-Cre* transgenic line (strain #014094, Jackson Laboratory) was used as a deleter line to generate the null allele. The characterization of this mouse model was described in detail elsewhere.[14]

Animals were housed according to IACUC recommendations. Both male and female mice were used in this study. Animals were generated by crossing *Bbs10*$^{+/-}$ males with either *Bbs10*$^{+/-}$ or *Bbs10*$^{-/-}$ females. Methods of euthanasia used were carbon dioxide inhalation followed by cervical dislocation. Humane endpoints were strictly observed, and every effort was made to minimize suffering.

Genotyping

Genotyping of *Bbs10* mice was performed using Taq polymerase (M0273, New England BioLabs) using the primers listed in Table 1 following the manufacturer's instructions. The 10 μL PCR reaction includes 2 μL of betaine. The cycling conditions consist of 5 min of initial denaturing step followed by 35 cycles of denaturing step at 94°C (30 s), the annealing step at 55°C (30 s), extension at 72°C (30 s), and then 2 min of final extension at 72°C. The size for the wild-type band in the PCR product is 445 bp, and for the knockout band is 260 bp.

AAV packaging and subretinal injection

The mouse *Bbs10* gene was cloned into a shuttle plasmid (#G0347) provided by the University of Iowa Viral Vector Core. This shuttle plasmid consists of the pFBAAV backbone, and contains a CMV promoter, multiple cloning sites, and a bovine growth hormone polyadenylation signal. This *Bbs10* expression cassette (Figure S3) was packaged into an AAV2/Anc80 viral vector (L65 variant)[19] by the Gene Transfer Vector Core at the Ocular Genomics Institute, Grousbeck Gene Therapy Center at Massachusetts Eye and Ear, Harvard Medical School. The formulation of the synthesized viral vector was 9.98×10^{12} genomic copies (gc)/mL, in PBS with an additional 35 mM NaCl and 0.001% PF68.

For subretinal injection, mice were anesthetized with a ketamine/xylazine mixture (87.5 mg/kg ketamine, 12.5 mg/kg xylazine). Subretinal injections were performed with a 32-gauge Hamilton syringe under a Zeiss OPMI f 170 surgical microscope. For AAV2/Anc80-*CMV-mBbs10*, two microliters of virus at 4×10^9 gc/μL concentration was injected into the temporal subretinal space of the mouse eye. The dilution buffer consists of 0.001% Poloxamer 188 Solution (P5556, Sigma Aldrich) in PBS (Gibco, # 10010-023), with addition of NaCl to make a total concentration of 190 mM NaCl. Subretinal treatment alternated between the right (OD) and left (OS) eyes for different cohorts of animals, and the contralateral eyes served as untreated controls. Wild-type or heterozygous mice were also treated with the viral vector to investigate any abnormal effects due to toxicity.

Fluorescence fundoscopy

Fluorescence fundoscopy was performed using the Phoenix MICRON III (Bend, Oregon) small animal imaging system. Mice were anesthetized using a ketamine/xylazine mixture (87.5 mg/kg ketamine, 12.5 mg/kg xylazine), and 1% tropicamide ophthalmic solution was applied for 3 min prior to the procedure. GONAK hypromellose ophthalmic demulcent solution (NDC 17478-064, Akorn) was applied on the eye prior to imaging.

ERG

Mice were dark adapted overnight. Mice were anesthetized using a ketamine/xylazine mixture (87.5 mg/kg ketamine, 12.5 mg/kg xylazine), and 1% tropicamide ophthalmic solution was applied for 3 min prior to the ERG procedure. GONAK hypromellose ophthalmic demulcent solution (NDC 17478-064, Akorn) was applied on the eyes prior to electrode placement. ERG was performed using the Celeris system from Diagnosys (Lowell, MA). To assess rod function, mice were subjected to dim flashes of 0.01 cd s/m^2 under dark-adapted conditions. Combined rod-cone function was measured by bright flashes of 3.0 cd s/m^2 under dark-adapted conditions. To assess cone function, mice were light adapted for 10 min to bleach rods in the retina. Then, two different measures, one involving isolated 3.0 cd s/m^2 bright flashes and the other using a train of 5-Hz flickering light, were used to evaluate the functions of cones. These tests are standardized ERG testing protocols established by the ISCEV.[42] Statistical analysis of ERG amplitudes was performed with GraphPad PRISM 9.0 using

two-way ANOVA. Values shown are averages ± standard error of the mean.

OCT

OCT was performed using the ONm600 system from Bioptigen (Research Triangle Park, NC). Mice were anesthetized using ketamine/xylazine mixture, and 1% tropicamide ophthalmic solution was applied for 3 min to dilate the pupils prior to the OCT procedure. Volumetric scans were taken centering on the optic nerves, as well as visualizing the peripheral regions of the retinas containing either the injection site or the equivalent areas in uninjected eyes. Peripheral side scans were acquired for both the temporal and the nasal regions of the eye, and, in these peripheral scans, the optic nerve was moved just outside the frame of imaging. Therefore, the imaging frames among different animals were comparable. Quantifications of ONL thicknesses in control and *Bbs10*$^{-/-}$ mice were performed at a position 500 μm away from the optic nerve head (temporal side) in the OCT center scans, and values between control and knockout mice were compared using Student's t test. For measuring ONL volumes in treated versus in untreated eyes, area of the entire ONL was manually segmented in each serial OCT image captured within the volumetric scan, and these ONL areas were multiplied by the scan thickness to derive the total ONL volume captured by that OCT volumetric scan (Figure S7). One OCT volumetric scan encompasses a circular area of the retina with a diameter of 1,400 μm. Quantification of ONL volumes were performed in scans focusing on either the central or peripheral retina containing the treated region in the treated eye of the animal, and in scans obtained at equivalent locations in the untreated contralateral eye of that animal. Values shown are averages ± standard error of the mean.

Visually guided swim assay

The visually guided swim assay, described in detail elsewhere,[14] was modified from the Morris water maze[43] and incorporated features of the mouse swim assay developed by Pang et al.[44] Briefly, mice were placed in a plastic swimming pool with a platform, whose position was randomly chosen for each trial. Mice were trained to visually identify, swim, and climb onto the platform. This swim assay was performed under two different lighting conditions, first under normal room light measuring 13.35 cd/m^2 (in a room with typical fluorescent ceiling lights) or in the dark assisted by dim red lighting measuring approximately 4.17×10^{-3} cd/m^2. The swim protocol consisted of four training days performed in the light, followed by four testing days in the light, then two training days in the dark, and finally four testing days in the dark. For each training or testing day, five swim trials were performed per animal. During each testing day of swimming, mice performed five swim trials to five different randomly selected platform locations. These platforms were the same for all mice in the test group. A limit of 60 s was set for each swim trial to prevent mice from becoming fatigued; if the platform was not attained by 60 s, the mouse was gently removed from the pool, and the time to platform for that particular trial was recorded as 60 s. Values shown are averages ± standard error of the mean.

Visualizing GFP using fluorescence microscopy

Whole mouse eyes were fixed in 2 mL of 4% paraformaldehyde/PBS for four nights at 4°C with gentle rotation and washed in PBS overnight at 4°C with gentle rotation. A puncture was made through the lens using a 26G syringe, and then the eyes were embedded in OCT freezing compound by placing it in a methybutane bath chilled with liquid nitrogen. The tissue blocks were stored at −80°C. The tissue blocks were sectioned at 10-μm thickness. Cryosections were permeabilized for 7 min using 0.3% Triton X-100 in PBS. Coverslips were placed after Vectashield mounting medium containing DAPI (Vector Laboratories) was applied to the sample, and these slides were imaged using a conventional fluorescence microscope.

Immunofluorescence microscopy

Mouse eyecups were collected and fixed following the protocol described earlier.[45] Briefly, eyecups were fixed in 4% (wt/v) paraformaldehyde/PBS for 3 h at 4°C after removal of anterior chamber and lens. Next, thoroughly washed eyecups were infiltrated and embedded in acrylamide as previously described.[45] Frozen embedded eyecups were mounted on a cryostat chuck in an orientation that sections became perpendicular to the retinal plane at the central retina. Eight-micrometer-thick serial sections were collected from the middle one-third of eyecups and used for immunohistochemistry.

Immunostaining and imaging procedures were performed as detailed earlier.[45] Briefly, sections were permeabilized with PBS-T (PBS, 0.1% Triton X-100), blocked in 5% (wt/v) BSA/5% (v/v) normal goat serum/PBS-T, and stained with indicated antibodies at room temperature for 3 h or at 4°C overnight. After rinsing, secondary antibodies conjugated to Alexa Fluor 488 or 568 (Life Technologies) were bound at room temperature for 2 h. After washing, Vectashield mounting medium containing DAPI (Vector Laboratories) was added, and images were taken using an Olympus IX71 microscope. Contrast enhancement was performed in the ImageJ software.

The following primary antibodies were used: anti-GFAP antibody (MAB3402, Chemicon), anti-GNAT2 antibody (ab 97,501, Abcam), anti-PRPH2 antibody (18109-1-AP, Proteintech Group), and anti-STX3 antibody (MAB2258, EMD Millipore).

DATA AND CODE AVAILABILITY

All data generated or analyzed during this study are included in this published article (and its supplementary information files).

SUPPLEMENTAL INFORMATION

Supplemental information can be found online at https://doi.org/10.1016/j.omtn.2022.12.007.

ACKNOWLEDGMENTS

The authors gratefully acknowledge the contributions of Dr. Darryl Nishimura. He will be dearly missed. The authors gratefully acknowledge Dr. Steve Murray (The Jackson Laboratory) for helpful discussions. The authors gratefully acknowledge the funding sources Fighting Blindness Canada, InVision 20/20, Bardet-Biedl Syndrome

Family Association, Ronald Keech professorship, NIH P30 EY025580, and Research to Prevent Blindness.

AUTHOR CONTRIBUTIONS

Conceptualization, A.D.; methodology, A.D., V.C.S., C.S., and L.H.V.; investigation, Y.H., S.B., J.T., A.M., S.K.M., J.M.T., P.D., J.G., and S.S.; visualization, Y.H.; funding acquisition, A.D. and V.C.S.; project administration, A.D.; supervision, A.D., Y.H., and S.B.; writing – original draft, Y.H. and A.D.; writing review & editing, A.D., V.C.S., S.S., L.H.V., C.S., J.G., P.D., J.M.T., S.K.M., A.M., J.T., S.B., and Y.H.

DECLARATION OF INTERESTS

L.H.V. is an inventor on patents that have been licensed to various biopharmaceutical companies and for which he may receive payments, including vector technologies herein described. L.H.V. is a paid advisor to Novartis, Akouos, and Affinia Therapeutics and serves on the Board of Directors of Affinia, Addgene, and Odylia Therapeutics, and he is an employee of ciendias bio. L.H.V. holds equity in ciendias bio, Akouos, and Affinia.

REFERENCES

1. Liu, P., and Lechtreck, K.F. (2018). The Bardet-Biedl syndrome protein complex is an adapter expanding the cargo range of intraflagellar transport trains for ciliary export. Proc. Natl. Acad. Sci. USA *115*, E934–E943. https://doi.org/10.1073/pnas.1713226115.
2. Ye, F., Nager, A.R., and Nachury, M.V. (2018). BBSome trains remove activated GPCRs from cilia by enabling passage through the transition zone. J. Cell Biol. *217*, 1847–1868. https://doi.org/10.1083/jcb.201709041.
3. Seo, S., and Datta, P. (2017). Photoreceptor outer segment as a sink for membrane proteins: hypothesis and implications in retinal ciliopathies. Hum. Mol. Genet. *26*, R75–R82. https://doi.org/10.1093/hmg/ddx163.
4. Datta, P., Allamargot, C., Hudson, J.S., Andersen, E.K., Bhattarai, S., Drack, A.V., Sheffield, V.C., and Seo, S. (2015). Accumulation of non-outer segment proteins in the outer segment underlies photoreceptor degeneration in Bardet–Biedl syndrome. Proc. Natl. Acad. Sci. USA *112*, E4400–E4409.
5. Hsu, Y., Garrison, J.E., Kim, G., Schmitz, A.R., Searby, C.C., Zhang, Q., Datta, P., Nishimura, D.Y., Seo, S., and Sheffield, V.C. (2017). BBSome function is required for both the morphogenesis and maintenance of the photoreceptor outer segment. PLoS Genet. *13*, e1007057. https://doi.org/10.1371/journal.pgen.1007057.
6. Swiderski, R.E., Nishimura, D.Y., Mullins, R.F., Olvera, M.A., Ross, J.L., Huang, J., Stone, E.M., and Sheffield, V.C. (2007). Gene expression analysis of photoreceptor cell loss in Bbs4-knockout mice reveals an early stress gene response and photoreceptor cell damage. Invest. Ophthalmol. Vis. Sci. *48*, 3329–3340. https://doi.org/10.1167/iovs.06-1477.
7. Nishimura, D.Y., Fath, M., Mullins, R.F., Searby, C., Andrews, M., Davis, R., Andorf, J.L., Mykytyn, K., Swiderski, R.E., Yang, B., et al. (2004). Bbs2-null mice have neurosensory deficits, a defect in social dominance, and retinopathy associated with mislocalization of rhodopsin. Proc. Natl. Acad. Sci. USA *101*, 16588–16593. https://doi.org/10.1073/pnas.0405496101.
8. Zhang, Q., Nishimura, D., Seo, S., Vogel, T., Morgan, D.A., Searby, C., Bugge, K., Stone, E.M., Rahmouni, K., and Sheffield, V.C. (2011). Bardet-Biedl syndrome 3 (Bbs3) knockout mouse model reveals common BBS-associated phenotypes and Bbs3 unique phenotypes. Proc. Natl. Acad. Sci. USA *108*, 20678–20683. https://doi.org/10.1073/pnas.1113220108.
9. Zhang, Q., Nishimura, D., Vogel, T., Shao, J., Swiderski, R., Yin, T., Searby, C., Carter, C.S., Kim, G., Bugge, K., et al. (2013). BBS7 is required for BBSome formation and its absence in mice results in Bardet-Biedl syndrome phenotypes and selective abnormalities in membrane protein trafficking. J. Cell Sci. *126*, 2372–2380. https://doi.org/10.1242/jcs.111740.
10. Mykytyn, K., Mullins, R.F., Andrews, M., Chiang, A.P., Swiderski, R.E., Yang, B., Braun, T., Casavant, T., Stone, E.M., and Sheffield, V.C. (2004). Bardet-Biedl syndrome type 4 (BBS4)-null mice implicate Bbs4 in flagella formation but not global cilia assembly. Proc. Natl. Acad. Sci. USA *101*, 8664–8669. https://doi.org/10.1073/pnas.0402354101.
11. Chandra, B., Tung, M.L., Hsu, Y., Scheetz, T., and Sheffield, V.C. (2022). Retinal ciliopathies through the lens of Bardet-Biedl Syndrome: past, present and future. Prog. Retin. Eye Res. *89*, 101035.
12. Stoetzel, C., Laurier, V., Davis, E.E., Muller, J., Rix, S., Badano, J.L., Leitch, C.C., Salem, N., Chouery, E., Corbani, S., et al. (2006). BBS10 encodes a vertebrate-specific chaperonin-like protein and is a major BBS locus. Nat. Genet. *38*, 521–524. https://doi.org/10.1038/ng1771.
13. Seo, S., Baye, L.M., Schulz, N.P., Beck, J.S., Zhang, Q., Slusarski, D.C., and Sheffield, V.C. (2010). BBS6, BBS10, and BBS12 form a complex with CCT/TRiC family chaperonins and mediate BBSome assembly. Proc. Natl. Acad. Sci. USA *107*, 1488–1493.
14. Mayer, S.K., Thomas, J., Helms, M., Kothapalli, A., Cherascu, I., Salesevic, A., Stalter, E., Wang, K., Datta, P., Searby, C., et al. (2022). Progressive retinal degeneration of rods and cones in a Bardet-Biedl syndrome type 10 mouse model. Dis. Model. Mech. *15*, dmm049473. https://doi.org/10.1242/dmm.049473.
15. Martin-Montalvo, A., Mercken, E.M., Mitchell, S.J., Palacios, H.H., Mote, P.L., Scheibye-Knudsen, M., Gomes, A.P., Ward, T.M., Minor, R.K., Blouin, M.J., et al. (2013). Metformin improves healthspan and lifespan in mice. Nat. Commun. *4*, 2192. https://doi.org/10.1038/ncomms3192.
16. Ladiges, W., Van Remmen, H., Strong, R., Ikeno, Y., Treuting, P., Rabinovitch, P., and Richardson, A. (2009). Lifespan extension in genetically modified mice. Aging Cell *8*, 346–352. https://doi.org/10.1111/j.1474-9726.2009.00491.x.
17. Grudzinska Pechhacker, M.K., Jacobson, S.G., Drack, A.V., Scipio, M.D., Strubbe, I., Pfeifer, W., Duncan, J.L., Dollfus, H., Goetz, N., Muller, J., et al. (2021). Comparative natural history of visual function from patients with biallelic variants in BBS1 and BBS10. Invest. Ophthalmol. Vis. Sci. *62*, 26. https://doi.org/10.1167/iovs.62.15.26.
18. Dilan, T.L., Singh, R.K., Saravanan, T., Moye, A., Goldberg, A.F.X., Stoilov, P., and Ramamurthy, V. (2018). Bardet-Biedl syndrome-8 (BBS8) protein is crucial for the development of outer segments in photoreceptor neurons. Hum. Mol. Genet. *27*, 283–294. https://doi.org/10.1093/hmg/ddx399.
19. Zinn, E., Pacouret, S., Khaychuk, V., Turunen, H.T., Carvalho, L.S., Andres-Mateos, E., Shah, S., Shelke, R., Maurer, A.C., Plovie, E., et al. (2015). In silico reconstruction of the viral evolutionary lineage yields a potent gene therapy vector. Cell Rep. *12*, 1056–1068. https://doi.org/10.1016/j.celrep.2015.07.019.
20. Tanimoto, N., Sothilingam, V., Kondo, M., Biel, M., Humphries, P., and Seeliger, M.W. (2015). Electroretinographic assessment of rod- and cone-mediated bipolar cell pathways using flicker stimuli in mice. Sci. Rep. *5*, 10731. https://doi.org/10.1038/srep10731.
21. Fernández-Sánchez, L., Lax, P., Campello, L., Pinilla, I., and Cuenca, N. (2015). Astrocytes and muller cell alterations during retinal degeneration in a transgenic rat model of retinitis pigmentosa. Front. Cell. Neurosci. *9*, 484. https://doi.org/10.3389/fncel.2015.00484.
22. Seo, S., Mullins, R.F., Dumitrescu, A.V., Bhattarai, S., Gratie, D., Wang, K., Stone, E.M., Sheffield, V., and Drack, A.V. (2013). Subretinal gene therapy of mice with bardet-biedl syndrome type 1. Invest. Ophthalmol. Vis. Sci. *54*, 6118–6132. https://doi.org/10.1167/iovs.13-11673.
23. Drack, A.V., Bhattarai, S., Seo, S., Stone, E.M., Sheffield, V., Mullins, R., and Tucker, B.A. (2014). Overcoming the overexpression toxicity of gene replacement therapy for Bardet Biedl Syndrome type 1. Invest. Ophthalmol. Vis. Sci. *55*, 4378.
24. Schneider, S., De Cegli, R., Nagarajan, J., Kretschmer, V., Matthiessen, P.A., Intartaglia, D., Hotaling, N., Ueffing, M., Boldt, K., Conte, I., and May-Simera, H.L. (2021). Loss of ciliary gene Bbs8 results in physiological defects in the retinal pigment epithelium. Front. Cell Dev. Biol. *9*, 607121. https://doi.org/10.3389/fcell.2021.607121.
25. Hsu, Y., Garrison, J.E., Seo, S., and Sheffield, V.C. (2020). The absence of BBSome function decreases synaptogenesis and causes ectopic synapse formation in the retina. Sci. Rep. *10*, 8321–8419. https://doi.org/10.1038/s41598-020-65233-4.
26. Jiang, J., Reho, J.J., Bhattarai, S., Cherascu, I., Hedberg-Buenz, A., Meyer, K.J., Tayyari, F., Rauckhorst, A.J., Guo, D.F., Morgan, D.A., et al. (2021). Endothelial

BBSome is essential for vascular, metabolic, and retinal functions. Mol. Metab. *53*, 101308.

27. Carvalho, L.S., Xiao, R., Wassmer, S.J., Langsdorf, A., Zinn, E., Pacouret, S., Shah, S., Comander, J.I., Kim, L.A., Lim, L., and Vandenberghe, L.H. (2018). Synthetic adeno-associated viral vector efficiently targets mouse and nonhuman primate retina in vivo. Hum. Gene Ther. *29*, 771–784. https://doi.org/10.1089/hum.2017.154.

28. Simons, D.L., Boye, S.L., Hauswirth, W.W., and Wu, S.M. (2011). Gene therapy prevents photoreceptor death and preserves retinal function in a Bardet-Biedl syndrome mouse model. Proc. Natl. Acad. Sci. USA *108*, 6276–6281. https://doi.org/10.1073/pnas.1019222108.

29. Seo, S., Zhang, Q., Bugge, K., Breslow, D.K., Searby, C.C., Nachury, M.V., and Sheffield, V.C. (2011). A novel protein LZTFL1 regulates ciliary trafficking of the BBSome and Smoothened. PLoS Genet. *7*, e1002358. https://doi.org/10.1371/journal.pgen.1002358.

30. Datta, P., Ruffcorn, A., and Seo, S. (2020). Limited time window for retinal gene therapy in a preclinical model of ciliopathy. Hum. Mol. Genet. *29*, 2337–2352. https://doi.org/10.1093/hmg/ddaa124.

31. Hsu, Y., Seo, S., and Sheffield, V.C. (2021). Photoreceptor cilia, in contrast to primary cilia, grant entry to a partially assembled BBSome. Hum. Mol. Genet. *30*, 87–102. https://doi.org/10.1093/hmg/ddaa284.

32. Mayer, S.K., Thomas, J., Helms, M., Kothapalli, A., Cherascu, I., Salesevic, A., Stalter, E., Wang, K., Datta, P., Searby, C., et al. (2022). Knockout of Bbs10 results in lack of cone electrical function and progressive retinal degeneration of rods and cones. Preprint at bioRxiv. https://doi.org/10.1101/2022.01.19.476952.

33. Pang, J.J., Chang, B., Kumar, A., Nusinowitz, S., Noorwez, S.M., Li, J., Rani, A., Foster, T.C., Chiodo, V.A., Doyle, T., et al. (2006). Gene therapy restores vision-dependent behavior as well as retinal structure and function in a mouse model of RPE65 Leber congenital amaurosis. Mol. Ther. *13*, 565–572. https://doi.org/10.1016/j.ymthe.2005.09.001.

34. Li, X., Li, W., Dai, X., Kong, F., Zheng, Q., Zhou, X., Lue, F., Chang, B., Rohrer, B., Hauswirth, W.W., et al. (2011). Gene therapy rescues cone structure and function in the 3-month-old rd12 mouse: a model for midcourse RPE65 leber congenital amaurosis. Invest. Ophthalmol. Vis. Sci. *52*, 7–15. https://doi.org/10.1167/iovs.10-6138.

35. Bennett, J., Duan, D., Engelhardt, J.F., and Maguire, A.M. (1997). Real-time, noninvasive in vivo assessment of adeno-associated virus-mediated retinal transduction. Invest. Ophthalmol. Vis. Sci. *38*, 2857–2863.

36. Bennicelli, J., Wright, J.F., Komaromy, A., Jacobs, J.B., Hauck, B., Zelenaia, O., Mingozzi, F., Hui, D., Chung, D., Rex, T.S., et al. (2008). Reversal of blindness in animal models of Leber congenital amaurosis using optimized AAV2-mediated gene transfer. Mol. Ther. *16*, 458–465. https://doi.org/10.1038/sj.mt.6300389.

37. Russell, S., Bennett, J., Wellman, J.A., Chung, D.C., Yu, Z.F., Tillman, A., Wittes, J., Pappas, J., Elci, O., McCague, S., et al. (2017). Efficacy and safety of voretigene neparvovec (AAV2-hRPE65v2) in patients with RPE65-mediated inherited retinal dystrophy: a randomised, controlled, open-label, phase 3 trial. Lancet *390*, 849–860. https://doi.org/10.1016/S0140-6736(17)31868-8.

38. Volland, S., Esteve-Rudd, J., Hoo, J., Yee, C., and Williams, D.S. (2015). A comparison of some organizational characteristics of the mouse central retina and the human macula. PLoS One *10*, e0125631. https://doi.org/10.1371/journal.pone.0125631.

39. Peterson, S.M., McGill, T.J., Puthussery, T., Stoddard, J., Renner, L., Lewis, A.D., Colgin, L.M.A., Gayet, J., Wang, X., Prongay, K., et al. (2019). Bardet-Biedl Syndrome in rhesus macaques: a nonhuman primate model of retinitis pigmentosa. Exp. Eye Res. *189*, 107825. https://doi.org/10.1016/j.exer.2019.107825.

40. Birch, D.G., Locke, K.G., Wen, Y., Locke, K.I., Hoffman, D.R., and Hood, D.C. (2013). Spectral-Domain optical coherence tomography measures of outer segment layer progression in patients with X-linked retinitis pigmentosa. JAMA Ophthalmol. *131*, 1143–1150. https://doi.org/10.1001/jamaophthalmol.2013.4160.

41. Hu, Z., Wang, K., Bertsch, M., Dunn, T., Kehoe, T., Kemerley, A.D., Helms, M., Bhattarai, S., Pfeifer, W., Scheetz, T.E., and Drack, A.V. (2019). Correlation between electroretinography, foveal anatomy and visual acuity in albinism. Doc. Ophthalmol. *139*, 21–32. https://doi.org/10.1007/s10633-019-09692-9.

42. McCulloch, D.L., Marmor, M.F., Brigell, M.G., Hamilton, R., Holder, G.E., Tzekov, R., and Bach, M. (2015). ISCEV Standard for full-field clinical electroretinography (2015 update) (vol 130, pg 1, 2015). Doc. Ophthalmol. *131*, 81–83. https://doi.org/10.1007/s10633-015-9504-z.

43. Morris, R. (1984). Developments of a water-maze procedure for studying spatial-learning in the rat. J. Neurosci. Methods *11*, 47–60. https://doi.org/10.1016/0165-0270(84)90007-4.

44. Pang, J.J., Boye, S.L., Kumar, A., Dinculescu, A., Deng, W., Li, J., Li, Q., Rani, A., Foster, T.C., Chang, B., et al. (2008). AAV-mediated gene therapy for retinal degeneration in the rd10 mouse containing a recessive PDE beta mutation. Invest. Ophthalmol. Vis. Sci. *49*, 4278–4283. https://doi.org/10.1167/iovs.07-1622.

45. Datta, P., Hendrickson, B., Brendalen, S., Ruffcorn, A., and Seo, S. (2019). The myosin-tail homology domain of centrosomal protein 290 is essential for protein confinement between the inner and outer segments in photoreceptors. J. Biol. Chem. *294*, 19119–19136. https://doi.org/10.1074/jbc.RA119.009712.